Analytical Methods

ROYAL SOCIETY OF CHEMISTRY

CRITICAL REVIEW

View Article Online
View Journal | View Issue

Cite this: *Anal. Methods*, 2023, **15**, 2154

The application of nanoparticles in point-of-care testing (POCT) immunoassays

Fengping Hou,[ab] Shiqi Sun,[a] Sahibzada Waheed Abdullah,[a] Yu Tang,[c] Xiongxiong Li*[b] and Huichen Guo*[ad]

The Covid-19 pandemic has led to greater recognition of the importance of the fast and timely detection of pathogens. Recent advances in point-of-care testing (POCT) technology have shown promising results for rapid diagnosis. Immunoassays are among the most extensive POCT assays, in which specific labels are used to indicate and amplify the immune signal. Nanoparticles (NPs) are above the rest because of their versatile properties. Much work has been devoted to NPs to find more efficient immunoassays. Herein, we comprehensively describe NP-based immunoassays with a focus on particle species and their specific applications. This review describes immunoassays along with key concepts surrounding their preparation and bioconjugation to show their defining role in immunosensors. The specific mechanisms, microfluidic immunoassays, electrochemical immunoassays (ELCAs), immunochromatographic assays (ICAs), enzyme-linked immunosorbent assays (ELISA), and microarrays are covered herein. For each mechanism, a working explanation of the appropriate background theory and formalism is articulated before examining the biosensing and related point-of-care (POC) utility. Given their maturity, some specific applications using different nanomaterials are discussed in more detail. Finally, we outline future challenges and perspectives to give a brief guideline for the development of appropriate platforms.

Received 4th February 2023
Accepted 5th April 2023

DOI: 10.1039/d3ay00182b

rsc.li/methods

1 Introduction

1.1 Necessity and significance of POC immunoassays

In recent years, increasing attention has been directed towards having a healthy, safe and convenient life, which is one of the most important issues in public health and life. However, all kinds of factors inevitably interfere with the health and safety of human beings, animals, and even food and the environment; for example, bacteria, viruses, fungi, and hazardous substances generated from biological sources and the surrounding environment, antibiotics, pesticides, and other additives. Traditional biological methods and wet chemistry assays require meticulous biological chemical conditions and sophisticated instruments, such as aseptic conditions, biological environments, high-performance liquid chromatography (HPLC), mass spectrometry (MS), HPLC-MS, gas chromatography (GC), atomic absorption spectroscopy (AAS), and flow cytometry.

Over the past three years, we have seen glimpses of the influence of COVID-19. The virus, COVID-19, is identified by advanced and sophisticated detection methods, mainly polymerase chain reaction (PCR) and whole genome sequencing, which have achieved great progress for microorganisms. There is no doubt that these methods are reliable and precise; however, the application of these methods is also limited to some extent by the requirements of a strict environment, specialized instruments, professional personnel and several hours for operation. This is one of the most important reasons why immunoassays are becoming the focus of attention. In a narrow sense, immune reactions take place *in vivo* between living pathogens and antibodies produced by organisms. With the development of immunology, the application has been broadened and immunoassays have been used to detect not only pathogens but also antibiotics, pesticides, and other molecules, which make it possible to realize point-of-care (POC) tests.

Thus, traditional detection methods are expanding to POCT diagnostics,[1] which go out of the laboratory and realize bedside testing-based approaches to address these challenges. The POCT assays should meet two application principles, namely, being user-friendly and as simple as possible so that anyone can learn to use them easily and understand how to interpret the results.[2] Selectivity, sensitivity and robustness are also some

[a]*State Key Laboratory of Veterinary Etiological Biology, OIE/China National Foot-and-Mouth Disease Reference Laboratory, Lanzhou Veterinary Research Institute, Chinese Academy of Agricultural Sciences, Xujiaping 1, Lanzhou 730046, Gansu, P. R. China. E-mail: guohuichen@caas.cn*

[b]*Lanzhou Institute of Biological Products Co., Ltd (LIBP), Subsidiary Company of China National Biotec Group Company Limited (CNBG), 730046 Lanzhou, China. E-mail: lixx985@163.com*

[c]*State Key Laboratory of Applied Organic Chemistry, Key Laboratory of Nonferrous Metal Chemistry and Resources Utilization of Gansu Province, College of Chemistry and Chemical Engineering, Lanzhou University, Lanzhou 730000, Gansu, P. R. China*

[d]*State Key Laboratory for Animal Disease Control and Prevention, College of Veterinary Medicine, Lanzhou University, Lanzhou Veterinary Research Institute, Chinese Academy of Agricultural Sciences, Lanzhou 730000, P. R. China*

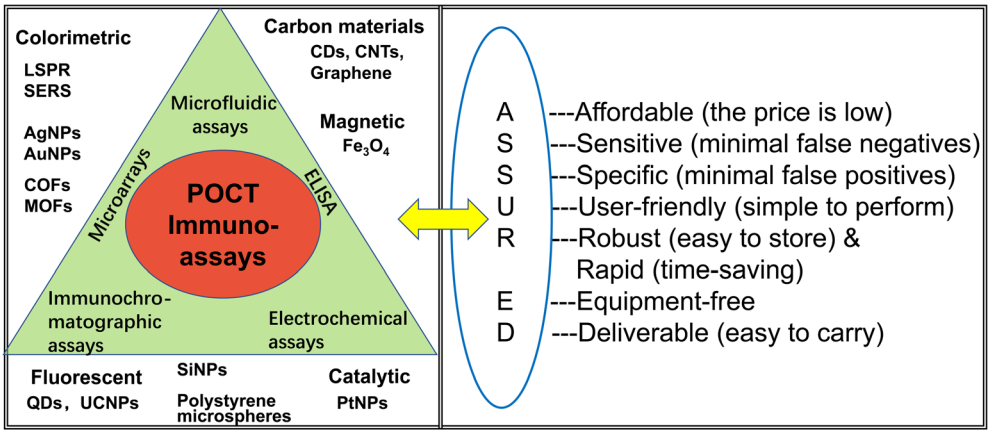

Fig. 1 The major POCT strategies and nanoparticles, and the interpretation of ASSURED criteria, WHO guidelines for the design of POCT assay.

important qualities for POC assays. As we know, the coronavirus was detected through PCR assays by a specialized agency for a long time, and then it was broadened to include antigen detection, a POCT assay, which can be operated by users. Therefore, it is necessary to realize that citizens can detect the antibody or antigen at home *via* a POC method.

To differentiate these POC immunoassays, we classified them into several types, namely, microfluidic immunoassays, electrochemical immunoassays (ELCAs), immunochromatographic assays (ICAs), enzyme-linked immunosorbent assay (ELISA), and microarrays (Fig. 1). There is a strong correlation between them but we have concentrated on different characteristics; for instance, ICAs are mainly paper-based lateral flow immunoassays with single channels, while microfluidic immunoassays are mainly about complex channels as compared to lateral flow immunoassays.

1.2 Overview of POC immunoassays

An early POC device was developed in 1957 when the urinalysis dipstick measured urinary protein using paper strips impregnated with pH indicator dyes.[3] Since the inception of modern microfluidics in the early 1990s, much research has focused on commercialized applications in POC technology.[4–6] POCT devices have several advantages, such as low consumption of reagents and samples, miniaturization of devices, and fast turnaround time for analysis. Rapid detection will drive rapid intervention, which is of crucial importance for disease diagnosis, especially for epidemic diseases.

Generally speaking, new POCT techniques aim to enhance three performance factors: (1) high throughput and low limit of detection (LOD), the detection of traces of targets from multiple clinical samples, (2) sensitivity and specificity, improving POCT's reliability and accuracy, and (3) the integration and automation of the POCT device to reduce labour, decreasing the sample-to-answer time, and eliminating operation errors due to manual procedures.[7]

The World Health Organization (WHO) has focused on POCT assays and some essential elements have been summarized as ASSURED criteria (Fig. 1) to evaluate these methods: affordability, sensitivity, specificity, user-friendliness (simple to perform in a few steps with minimal training), robust and rapid (results available in less than 30 min), equipment-free and deliverable to those who need them.[8–10] Specifically, the criteria were developed as a benchmark to judge whether the diagnostic assays address the requirement for resource-constrained settings.[11] However, it is difficult to meet all of these criteria; therefore, the development of excellent POCT platforms to maximize the requirements is still challenging.

A prime example is the glucose assay, which is a well-established leader in the commercial field of POCT. Like blood glucose meters, the majority of early commercial self-test platforms are electrochemical, based on the redox-couple-mediated enzymatic oxidation of glucose to produce a catalytic electrochemical current.[3] With the demand for new POC diagnostic technologies, there has recently been much interest in developing novel and clever methods to re-purpose POCT devices, to significantly improve their performance and expand their detection range of targets.

Immunoassay is based on specific binding between antibody-antigen pairs. Fig. 2 shows two common types of

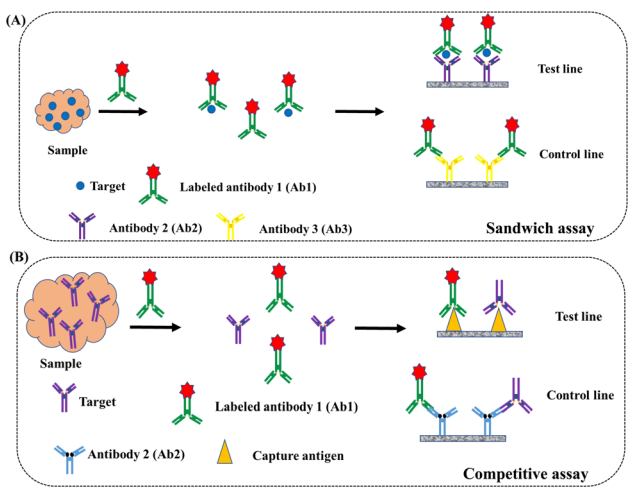

Fig. 2 Scheme of (A) sandwich and (B) competitive immunoassays.

Table 1 Some typical examples of immunoassays utilizing different nanoparticles[a]

Detection method	NPs	Analyte	Limit of detection	Time	Remarks	Ref.
LFA & CMA	AuNPs	IgG antibodies against the Ebola virus	200 ng mL^{-1}	15 min	AuNPs were functionalized with a secondary antibody to bind with recombinant virus at the test line	73
LFA & CMA	AuNPs	DNA	2.5 μg mL^{-1} (1.25 fM)	15 min	The nucleic acid biosensor was labelled with horseradish peroxidase (HRP)-Au-NP to detect human genomic DNA	67
LFA & SERS (Raman)	Au/Au core/satellite nanoparticles	hCG	1.6 mIU mL^{-1}	—	The SERS-labeled anti-hCG antibodies were mixed with serum samples. The corresponding sandwich complex with the capture Ab can form at the test line. The signal was read by Raman microscopy with point illumination	79
LFA & fluorescence	AuNPs-Cy5	CEA	5.89 pg mL^{-1}	10 min	Antibody (Ab1)-decorated AuNPs immigrated to the control line along with the sample and captured antibody (Ab2)-decorated Cy5 printed as fluorescent probes to form a sandwich-like reaction, resulting in reverse fluorescence enhancement and colorimetric bimodal signal readout	160
LFA & CAA	Pt–Au nanoparticles	*E. coli* O157:H7	100 cells per mL	20 min	3,3′,5,5′-Tetramethylbenzidine (TMB) was catalyzed by Pt–Au NPs, producing a blue-colored product that served as a good signal amplifier to realize the visualization and quantification of the target pathogen	129
LFA & fluorescence	Europium microspheres	Silk fibroin	8.09 ng mL^{-1}	25 min	Lanthanide-labeled anti-silk fibroin antibody to detect silk fibroin	155
LFA & TRFIA	Europium nanospheres	Aflatoxin	0.16 μg kg^{-1}	12 min	The carboxylated polystyrene nanospheres doped with europium were conjugated with anti-aflatoxins antibody to form a time-resolved fluorescence immunoassay	154
LFA & up-conversion fluorescence	UCNPs	*Yersinia pestis*, *Burkholderia pseudomallei*	100 CFU per test, 1000 CFU per test	15 min	$NaYF_4$:Yb^{3+}, Er^{3+} UCNPs codoped with Li^+ and K^+ were functionalized with amino groups and then conjugated with antibodies through the glutaraldehyde bridge. Two monoclonal antibodies were sprayed as two test lines, and dual-target UCNP strips for the simultaneous detection of *Y. pestis* and *B. pseudomallei*	141
LFA & fluorescence	Quantum dot beads	Aflatoxin B1	0.42 pg mL^{-1}	15 min	CdSe/ZnS was encapsulated by a microemulsion technique to form quantum dot beads (QBs). The QBs were conjugated with anti-AFB1 mAbs through the EDC-activated intermediate	111
ELCA	Carbon electrodes coated with AuNPs	N-Protein	0.4 pg mL^{-1} in PBS	15 min	The electrodes were functionalized using 11-mercaptoundecanoic acid to immobilize the antibody against N-protein	65
ELCA & field-effect transistor (FET)	Graphene	Spike protein	1.6×10^1 pfu mL^{-1}, 2.42×10^2 copies per mL	—	The probe was produced by coating graphene sheets of the FET with a specific antibody against the SARS-CoV-2 spike protein	169

Table 1 (*Contd.*)

Detection method	NPs	Analyte	Limit of detection	Time	Remarks	Ref.
ELISA	Fe_3O_4 nanoparticle, gold nanozymes	H1N1	5.0×10^{-12} g mL^{-1}	—	Combining the silica-shelled magnetic nanobeads and gold nanozymes to separate targets and amplify the signal	124
ULISA	UCNPs	Diclofenac	0.05 ng mL^{-1}	>1 h	UCNPs were coated with a silica shell exposing carboxylic acid. COOH-UCNPs were then conjugated to a secondary anti-IgG antibody *via* standard EDC/sulfo-NHS chemistry	61
Microfluidic assay	Mechanically induced trapping of molecular interactions	IgG and IgM levels against four SARS-CoV-2 proteins	1.6 ng mL^{-1}	—	Mechanically induced trapping of molecular interactions serves as a fluorescence biosensor where indirect immunoassays for each of the four viral antigens are performed	40
Microfluidic assay	Silver nanocubes	Cytokine	0.46–1.36 pg mL^{-1}	<100 min (8 samples)	One-step sandwich immunoassay with three notable features: (i) a microfluidic microarray patterning technique for high-throughput, multiantibody-array biosensing chip fabrication; (ii) an ultrasensitive nanoplasmonic digital imaging technology utilizing 100 nm silver nanocubes (AgNCs) for signal transduction; (iii) rapid and accurate machine-learning-based image processing method for digital signal analysis	33
Microarray	Titanium oxide (TiO_2)	Extracellular vesicles (EVs)	2.18×10^9 EVs per mL	<2 h	The microarray platform, which consists of an array of antibodies printed on a photonic crystal biosensor and a microscopic hyperspectral imaging technique, can rapidly assess the binding of the EV membrane proteins with their corresponding antibodies	63

[a] Lateral flow assays (LFA); colorimetric assay (CMA); surface-enhanced Raman scattering (SRS); fluorescence immunoassay (FLIA); fluorescence enzyme-linked immunosorbent assay (FELISA); catalysis assay (CAA); upconversion-linked immunosorbent assay (ULISA); time-resolved fluoroimmunoassay (TRFIA); electrochemical assay (ELCA).

immunoassays, namely, the sandwich-like immunoassay and the competitive immunoassay. The sandwich immunoassay is the most common one, in which the target analytes in the test sample are captured by the affixed antigens or antibodies, and further, bind to the labeled molecules. The number of analytes in the test sample is relevant to the number of labeled molecules in this format. In a competitive immunoassay, an unlabeled analyte (with targeting antibody, Ab, as an example) in the test sample is measured due to its ability to compete with the pre-labeled antibody (Ab*). The unlabeled antibody competes with the labeled antibody to bind the affixed antigen; thus, the antibody in the test sample is inversely related to the amount of labeled antibody measured in the competitive format.

Recently, the development of nanomaterials and nanotechnology has promoted the progress of POCT platforms, which have been widely used in colorimetric,[11] optical,[12] electrochemical,[13] magnetic,[14] and catalytic[15] approaches. The POC platforms have been used to detect nucleic acids,[16] proteins,[17] pesticides,[18] viruses,[19] bio-markers in disease diagnosis,[20,21] and even heavy-metal species.[22–24] As we know, there are some shortcomings in conventional immunolabelling including immunofluorescence, radioimmunoassay, and enzyme labeling technology. Fluorescent dyes and microorganisms with fluorescence are also used for immunofluorescence labelling; however, their fluorescence is easily quenched and/or strict storage conditions are used. Because of the expensive instruments and safety hazards, radioimmunoassay is hard to promote. Though enzyme labeling technology has been widely used, the sensitivity needs to be improved. Nanoparticles can be used to improve these drawbacks. On the one hand, nanoparticles can provide a large amount of space for loading dyes and surface modification, and various molecules can be attached to control their physical and chemical properties. On the other hand, the special characterisations of optical, magnetic, electrical and thermal properties enable them to play different roles in immunoassays, such as fluorescence

donators, separation, carriers, protective agents, and so on. Thus, the sensitivity and stability are improved.

A comparison of different immunoassays based on nanoparticles is made in Table 1, in which the sensing scheme for individual nanoparticles, and the uniqueness of each nanomaterial are described. The POCT assays have been used for detection in all kinds of analysis, including proteins, nucleic acids, toxins, small molecules, antibodies, and even bacteria.

2 Different platforms of POCT immunoassays

2.1 Microfluidic immunoassays

Generally speaking, microfluidic-based platforms provide a set of fluidic unit operations that allow the implementation of complete chemical or biological processes conveniently and flexibly; for example, sample collection, preparation, reaction and analysis.[25,26] These platforms have been investigated for accurate fluid control, which can offer miniaturization, integration, automation and parallelization of the reaction process.[27] Microfluidic platforms have many advantages: (1) low fluid volume consumption. The volume of fluid can be varied from femtoliters to microliters, leading to less waste, lower reagent costs and less sample volume for reaction. (2) Rapid response and result output, even down to milliseconds, due to high surface-to-volume ratios, short diffusion distances and small capacities. (3) Safer operation processes because of the integration of multiple functionalities and less sample and reagent exposure. (4) Easy operation allows the devices to be used *in situ* without trained experts. (5) The simultaneous detection of multiple samples using multiple channels.

The microfluidic platforms have been divided into five groups according to the primary liquid propulsion resource:

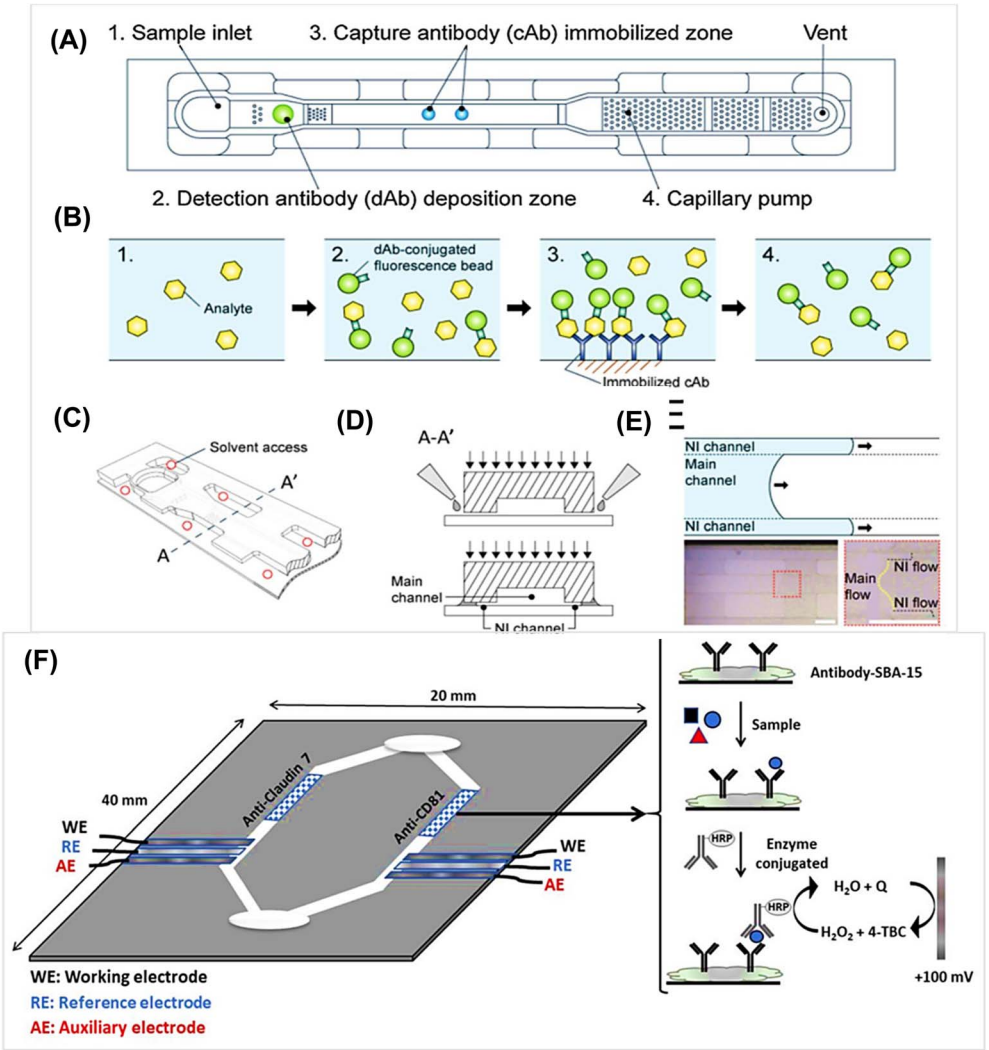

Fig. 3 Microfluidic immunoassay. Schematic illustration of (A) the microfluidic device comprising immunoassay elements and (B) interactions between antibodies and analytes along the sample flow. (C) Structure showing solvent access for the assembled device. (D) Cross-sectional view of the nanointerstice (NI) channel generated by solvent bonding (A–A′). (E) The air–liquid interface (ALI) in the channel filling flow. Reproduced with permission from Kim *et al.*, *Sens. Actuators B Chem.*, 2020, **316**, 128094. Copyright 2020, Elsevier. (F) Schematic representation of the electrochemical paper-based immunosensor for Claudin 7 and CD81 dual determination. Reproduced with permission from Ortega *et al.*, *Anal. Chem.*, 2021, **93**, 1143–1153. Copyright 2021, American Chemical Society.

capillary, pressure-driven, centrifugal, electrokinetic and acoustic systems.[26] It is well known that lateral flow assay is based on capillary action, and the electrokinetic system is closely related to the electrochemical assay. The pressure-driven system includes several types, for instance, linear actuated devices, pressure-driven laminar flow, microfluidic large-scale integration and segmented flow microfluidics. The centrifugal-based microfluidic platforms are also integrated with a loop-mediated isothermal amplification (LAMP) system for detecting nucleic acids.[28,29] Herein, we mainly introduce the microfluid assays, which emphasize the channel design and microfluid process, and there is relatively less focus on the nanoparticles.[30,31]

Recently, much attention has been paid to the development of microfluidic-based platforms for biological analysis. Fig. 3A–F shows microfluidic devices and the performance of related elements. The devices consist of five regions: sample inlet, detection antibody (dAb) zone, capture antibody (cAb) zone, capillary pump, and vent hole.[30,32] The thermoplastics, such as poly (methyl methacrylate) (PMMA), are common substrates used in microfabrication. The fluorescence beads are preloaded with detection antibody, which can react with the analyte H1N1 Influenza A during channel flow. Although a mass-producible antibody dotting technique for influenza A was developed, the limit of detection (LOD) was not improved as compared with the conventional sandwich fluorescence immunoassay method.

In another illustrative example, AuNPs were coated with anti-β-2-microglobulin and a special microfluid cuvette was designed.[32] The signal record was through the aggregation of AuNPs to produce the observable color and signal of localized surface plasmon resonance (LSPR) of AuNPs. Silver nanocubes are also used in nanoplasmonic digital imaging technology for signal transduction.[33] The 100 nm silver nanocubes were synthesized according to the seed-mediated growth procedure, and a multi-capture antibody microarray chip was fabricated using a microfluidic flow-patterning technique. The developed immunoassay allowed the simultaneous detection of six cytokines in a single run with wide working ranges and ultralow detection limits. Some researchers combined self-coalescence module (SCM) and capillary assembled receptor carriers to remould the traditional lateral flow technology.[34] They used silicon-based beads functionalized with capture antibodies to form a bead lane module, resulting in using low volumes of sample and reagent and a controllable process. A washing-free centrifugal microchip fluorescence immunoassay was also developed, in which a fluorescent microsphere-labeled capture antibody and matrix nano-spotting technology were employed to immobilize antibodies on the surface of the microchips.[35] Fluorescent streptavidin PMMA beads were also utilized as substrates to integrate the antibody (Ab1) into microfluidic chips, and gold nanoparticles-conjugated antigens and antibodies (Ab2) accumulated on the beads and were further stained with silver, resulting in the attenuation of the fluorescence signal of fluorescent beads.[36] Immunomagnetic beads were also used to detect prostate specific antigen with an integrated magnetic microfluidic platform.[37]

To enhance the stability of the bead-based digital microfluidic immunoassay, the amounts of magnetic beads were investigated.[38] The results showed that it became difficult to aggregate in the microfluidic immunoassay chip when the bead numbers were too high or too low. Therefore, each link should be optimized for the assay and full use should be made of the advantages of the high-throughput detection of the microfluidic immunoassay. The spread of Covid-19 makes it particularly important that the latest biosensor technologies for general human use should be environmentally friendly and also provide a lot of information on the spread of disease and preventive controls.[39,40]

2.2 Electrochemical assays (ELCAs)

The electrochemical assay is currently being developed for potential POC testing. The reason it attracts wide attention is that the devices are low-cost and miniature. However, electrochemistry also has some fundamental terms and basic principles, which make the process a bit complicated. Electrochemical methods, such as linear sweep, square-wave, differential pulse and stripping, also use voltammetry and amperometry to detect protein biomarkers.[13] Generally, the production of an electrochemical signal needs a cell consisting of three electrodes: a working electrode (WE), a counter electrode (CE) and a reference electrode (RE) (Fig. 3F). The redox reactions of interest occur on the WE; the WE potential and balance current are set by the CE controlled through the potentiostat, and the WE potential is fed to the potentiostat through the RE.[41] Therefore, electrodes are the most important parts of ELCAs and much attention has been paid to electrode material, size and surface structure.

The work process is as follows: first, tracer antibodies or antigens are labeled with enzymes or nanoparticles as electroactive species; second, the target analyte is allowed to be captured by the tracer and immobilized on an electrode surface, in which an intermediate antibody may need to participate; third, the potential or current at the electrode is detected, which is relative to the concentration of the analyte. In this process, when the targets exist, they bind with the tracer and the redox reaction simultaneously produces a potential or current signal that is proportional to the concentration of the analytes. The glucometer is commonly used and it is a typical representation of the utilization of the electrochemical modality.[42,43] Focus has shifted to simplifying the operation procedure and reducing the detection time rather than just pursuing sensitivity and accuracy, and thus a convenient assay has become one of the most effective ways to develop electrochemical biosensors.[44]

Signal amplification is the key to designing high-performance immunoassays for analytes, especially in complex samples with a low abundance of targets. Three strategies, enzyme-based, nanomaterial-enhanced, and DNA-based signal amplification, have been applied to accomplish this process.[45] Enzyme-based immunoassays are the most common high-efficiency methods owing to the fast and selective catalytic activity; therefore, enzymes are the most valuable labels in biology, such as horseradish peroxidase (HRP), alkaline

phosphatase (ALP), acetylcholine esterase (AChE) and glucose oxidase (GOx).[46] Nanomaterials, especially carbon-based nanomaterials and noble metal nanoparticles, have been used for signal amplification. On the one hand, they are excellent electrode materials; on the other hand, they are similar to a natural peroxidase, for example, platinum, gold, silver and other metal oxides show excellent catalytic ability toward hydrogen peroxide. DNA-based amplification introduces current DNA nanotechnology signal amplified strategies.

Metal-based nanoparticles are the most popular electrode materials apart from carbon materials because these metal nanoparticles, such as gold, silver, platinum and copper, have special optoelectronic properties that are dependent on their unique sizes and shapes.[47] The high surface area and capacity for surface modification make them easily tunable optical properties. Apart from their excellent conductivity, these metal nanoparticles have been explored as catalysts due to their superior stability and redox capacity. Some essential principles cannot be neglected, such as hypotoxicity, convenient fabrication process and non-interference with other labels. Based on all of these, noble metal nanoparticles have been proven to be among the most important groups of nanomaterials for POC biosensing approaches, as well as in other biomedical therapeutic applications. Some non-noble-metal oxygen evolution reactions nanocatalysts have also been developed as electrocatalytic labels. The application of $NiCoO_2$@CeO_2 nanoboxes for Interleukin-6 detection was reported.[48] Fernández-Baldo *et al.* designed an electrochemical paper-based immunoassay for Claudin 7 and CD81 dual determination, in which mesoporous silica particles SAB-15 were used to capture antibodies and rGO was used to modify electrodes.[49] Quantitative POC devices for serological disease diagnosis have attracted significant attention in the last few years. As an example, a potentiometric sensor based on extended-gate field-effect transistors in a dual-chip configuration were developed.[50] Nanobodies are a unique antibody fragments, which have small molecular weight, and simple structures and can be easily cloned and modified genetically. It has been reported that nanobodies were immobilized with AuNPs and TiO_2 spheres to determine SARS-CoV-2 viral pathogens.[51] The immunoassay of the SPR effect of AuNPs combined with nanobodies realized satisfactory sensitivity, stability, and reproducibility. All of these perspectives further broaden the applications of immune platforms.

The goal of ELCA is to achieve accurate, continuous target detection and the simultaneous detection of multiple targets in complex samples. Though great progress has been achieved in this field, the goal has not been reached. Therefore, massive efforts have to be spent on the platform to realize real POC assays. To obtain more sensitive responses, higher reproducibility and a wider working range, the technology of ELCA has to be combined with microfluid assay and further extended to multiplexed detection in a single device.[52]

2.3 Immunochromatographic assays (ICAs)

Immunochromatographic assays (ICAs) use membrane or paper strips to indicate infectious diseases and the abuse of drugs,

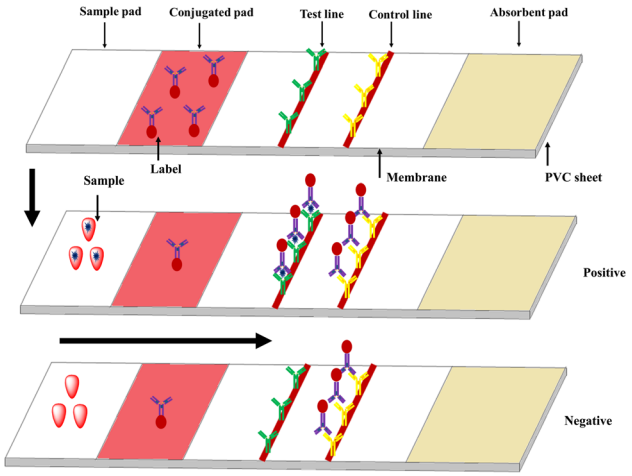

Fig. 4 Typical immunochromatographic assay format.

and even the presence of protein markers such as pathogen antigens and host antibodies. The ICA devices incorporate porous membranes, antigens and/or antibodies, and a signal-generating system, which relies on fluid migration technology as outlined in Fig. 4. A classic example is human chorionic gonadotropin (hCG) testing strips. The immune reaction proceeds on the strips and the results are judged by observing the color of gold nanoparticles using the naked eye. The immunochromatographic testing strips (ICTSs) have lots of advantages such as being portable and time-saving, with low cost, convenient operation and observation by the naked eye. However, the strips also have some shortcomings, such as qualitative or semi-quantitative detection, liquid sample with low viscosity and false positive or false negative results. At present, ICTSs are used to detect disease pathogens (bacteria, viruses, and relative disease markers),[53,54] environmental contaminants,[55] food additives,[56,57] and veterinary drugs,[58] and have been extended beyond proteins and glucose.[59] Even though there are several reviews about ICAs that have been reported in the past decades,[60] a large number of novel materials, technology and methods have not been covered. Herein, for greater clarity, we explain from the nanoparticles point of view.

2.4 ELISA

ELISA and real-time PCR are candidates for simultaneous quantification with high sensitivity, however, they are expensive for use in clinical diagnosis. These techniques need further development before they can be employed as bed-side POCT assays. As a detection platform, ELISA has several merits, including lower cost, less reagent consumption, and simplicity of operation as compared with real-time qRT-PCR. It is well-known that ELISA uses an immunoassay for detecting targets according to the antibody-antigen interaction as well as catalyst-based signal transduction. Conventional ELISA has been modified by different optical materials and catalysts, including AuNPs, and organic dyes. Alternatively, the catalysis of hydrogen peroxide can be used to promote trace analyte

detection, in which enzymatic reactions are generated from acetylcholinesterase-catalyzed hydrolysis or alkaline phosphatase catalysis.

Gorris *et al.* prepared carboxyl-silica-coated UCNPs, which were conjugated to a secondary anti-IgG antibody as the label, enabling the sensitive detection of diclofenac (DCF).[61] Benefiting from the free background signals caused by the special anti-Stokes luminescent probes, UCNPs have been utilized in ICA and ELISA to sensitively detect bacteria, viruses, antibiotics and mycotoxins.[62] The results also demonstrated that UCNPs are suitable for multiplex analysis for complex samples and display remarkable effects.

2.5 Microarrays

Microarrays also use sandwich immunoassay according to the antigen–antibody interaction just like ELISA. Microarray approaches for target detection boast high throughput and sensitivity after integration with RT-PCR to amplify the signal of a fluorescent tag from a trace analyte.

Microarrays or microwells demonstrate desirable characteristics to run multiplex POC assays. Compared with ELISA, microarray POCTs decreased analysis time (1 h), reduced reagent use, and required a smaller sample volume (5 μL). Paper- or poly-diacetylene-based microarrays can produce colorimetric or fluorescent visually-readable signals that can be

Table 2 Summary of representative engineered nanomaterials used in POCT assays

Nanoparticles	Characteristics	Analyte	Biosensor type	Ref.
AgNPs	Strong surface plasmon resonances (SPR) under incident light; offer the highest conductivity and reflectivity and display size-dependent catalytic activity among all metals	HBV, HIV	Optical/electrochemical	71
AuNPs	Possess unique LSPR characteristics with high molar extinction coefficients, exhibit aggregation or disaggregation-based chromogenic changes in the presence of the targeted analytes due to the variation in their size	HPV, HIV	Optical/electrochemical	19
Quantum dots (QDs)	QDs are nanosize particles with unique optical and electrical properties and are powerful tools for providing rapid and sensitive virus detection to facilitate early treatment and monitoring of viral disease	HBV, HIV	Optical/electrochemical	100
Magnetic nanoparticles (MNPs)	Controllable by an external magnet; super-paramagnetic properties can separate specific molecules from complex samples under a mild magnetic field to decrease the matrix interference; act as transducers, catalysts as well as complexing agents for magnetic enrichment	LAV, HBV	Electrochemical	114
Pt-NPs	With their high surface area, diverse composition and excellent electron conductivity, they show high catalytic activity and stability and are superior to natural enzymes, form core–shell structures, or form an electrode	*E. coli*	Electrochemical	127
UCNPs	Under NIR excitation, UCNPs can generate the anti-Stokes process, where two or more low-energy photons are converted to high-energy output photons	Myoglobin, Yersinia pestis	Optical/fluorescence	142
SiNPs	With large pore channels and highly accessible inner surfaces, SiNPs have been used as nanocarriers for drugs, dyes and biomacromolecules. Molecules can be attached to the surface or enter holes of the SiNPs	HBV, HPV	Optical	152
Polystyrene microspheres	Polymer materials formed through the reaction of styrene; owing to robustness and easy functionalization with carboxyl, they are widely used to load fluorescent materials as carriers	Silk fibroin, *E. coli*	Optical/fluorescence	159
Carbon nanotubes (CNTs)	CNT-based biosensors possess high selectivity and sensitivity due to their high surface area; this platform is also useful because of their ease of functionalization	HBV, HPV	Electrochemical	164
Graphene oxide (GO)	The size controllability of GO nanosheets and changes in their oxidation level are unique features for this biosensor platform to detect specific viruses	HBV, HIV	Optical/ electrochemical/ potentiometric	170
MnO_2 nanosheets	MnO_2 nanosheets possess oxidase-like activity that can catalyze the oxidization of TMB. Meanwhile, the existence of GSH can cause the reduction of oxidized TMB, which will generate a visual color change	Glutathione	Electrochemical/ catalyst	177
ZnO	With piezoelectric properties, ZnO plays a main role in special sensors known as mechanochemicals	HIV	Electrochemical	64
Aluminum (AINPs)	The nanoporous morphology of AINPs is the most prominent and attractive feature for designing biosensors; porous structure enhances the surface-to-volume ratio that results in an increased number of target molecules inside pores	DENV, Ebola	Electrochemical	147

read using a smartphone's camera.[7] An extracellular vesicle (EVs) microarray was reported to discriminate EVs released by closely related cell types.[63] The EV assay used the label-free optical sensing mechanism for multiplexed analysis, and the microarray platform increased the throughput *via* the simultaneous characterization of multiple immunobinding reactions.

3 Nanoparticles for POCT immunoassays

Nanoparticles with different strategies result in different detection limits due to the sensitivity of the detecting system. The difference can be attributed to multiple factors, for example, the validation of target analytes, signal amplification mode, the protocols for separation and integration of samples, the sensing interfaces and modification conditions, minimal interference, and cost-effectiveness. These factors can be resolved by integrating novel nanomaterials-assisted signal amplification technology into the immune systems for target diagnosis. Table 2 shows the main nanoparticles used in POCT assays, describing the uniqueness of each type of nanoparticle.[64]

The methods of combining nanoparticles and probes are summarized in the following: (1) for noble metal particles, such as AgNPs and AuNPs, there are several existing interactions between nanoparticles and proteins, which include hydrogen bonds, hydrophobic interactions, electrostatic interactions and dative bonds (Fig. 5A). (2) Nanoparticles with carboxyl groups are activated by EDC and NHS, and then combined with amino groups of proteins or other biomolecules (Fig. 6A).[65] (3) For nanoparticles with amino groups, they are combined with the amino groups of proteins or other biomolecules *via* glutaraldehyde linkages (Fig. 6B). (4) For some nanoparticles with macropores, such as SiNPs, the biomolecules easily enter the pores and are protected by other interactions mentioned in the first point (Fig. 6D). (5) For some nanoparticles with strong absorption capacity, such as GO, carbon nanotubes and titanium dioxide materials, biomolecules are absorbed by the materials (Fig. 6F). Here, we make a classification to elaborate on how to link nanoparticles to the probes; the interactions do not exist alone.

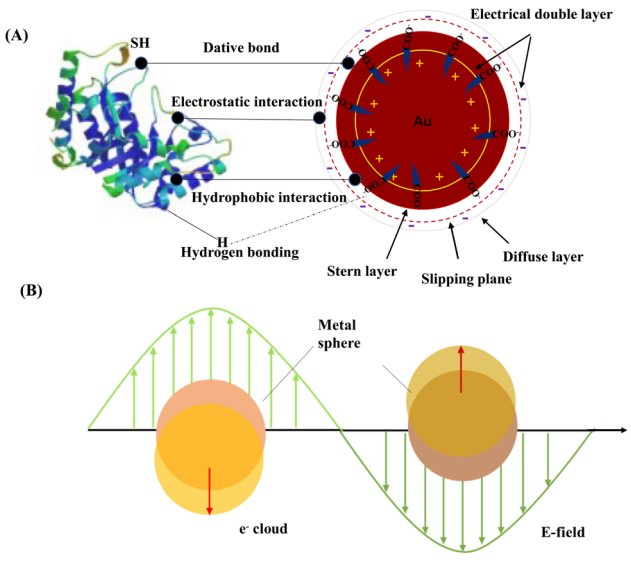

Fig. 5 The chemical binding principle of AuNPs conjugated with proteins. Figure adapted from Chou, *Analyst*, 2013, **138**, 2620–2623. (B) Schematic illustration of a localized surface plasmon. Figure adapted from Kelly *et al.*, *J. Phys. Chem. B*, 2003, **107**, 668–677. The electric field induces polarization of the free electrons on the surface of the metal spheres.

3.1 Metal-based inorganic nanoparticles

The colorimetric assay is of great practical significance in POC testing as the analysis of the readout results requires neither a sophisticated instrument nor a technician; thus, it is nearly the most convenient platform for detecting a wide variety of analytes. Colored nanoparticles have been used to detect lots of common molecules and biomarkers, for instance, human IgG for virus detection in serum,[66] human genomic DNA,[67] C-reactive protein (CRP) concentrations in human serum,[68] carcinoembryonic antigen (CFA),[69] and even eleven benzimidazoles in a milk sample by one monoclonal antibody.[70] Researchers have been devoted to developing different NPs and various sensor platforms to realize the sensitive detection of targets.

3.1.1 Silver nanoparticles (AgNPs). Though AgNPs are not as widely investigated as AuNPs, they have a significant influence on the field of nanoscience. As is well known, silver is widely used as an antimicrobial. AgNPs are technologically important materials; to be more specific, they offer the highest conductivity and reflectivity and display size-dependent catalytic activity among all metals.[71]

Just like AuNPs, AgNPs present strong surface plasmon resonances (SPR) under incident light. The AgNPs have high extinction coefficients as compared to AuNPs of similar size and are valuable for a variety of colorimetric/optical sensors. In addition, Raman scattering and fluorescence signals are significantly enhanced on the surfaces of various silver nanostructures, which can serve as highly sensitive optical sensing probes.[71] Moreover, AgNPs can be oxidized more easily than AuNPs and offer excellent electrochemical activity, resulting in their great potential in electrochemical sensing.[72] AgNPs-based assays have been widely developed, including electrochemistry, silver-enhanced fluorescence, surface-enhanced Raman scattering, colorimetry and chemiluminescence.[73] However, because of their instability and difficulty of functionalization, AgNPs attract much less attention than AuNPs.

The color change of AgNPs is related to the surface plasmon absorption band, which is dependent on several parameters such as the size, shape, capping agent, medium refractive index, and state of AgNPs.[74] Recently, the application of AgNPs has been increasing with the development of synthesis and functionalization methods for AgNPs. Choi *et al.* introduced a facile and novel fabrication method, in which the nanoparticles were directly synthesized within the paper without external processing.[75] This approach is based on the successive ionic layer

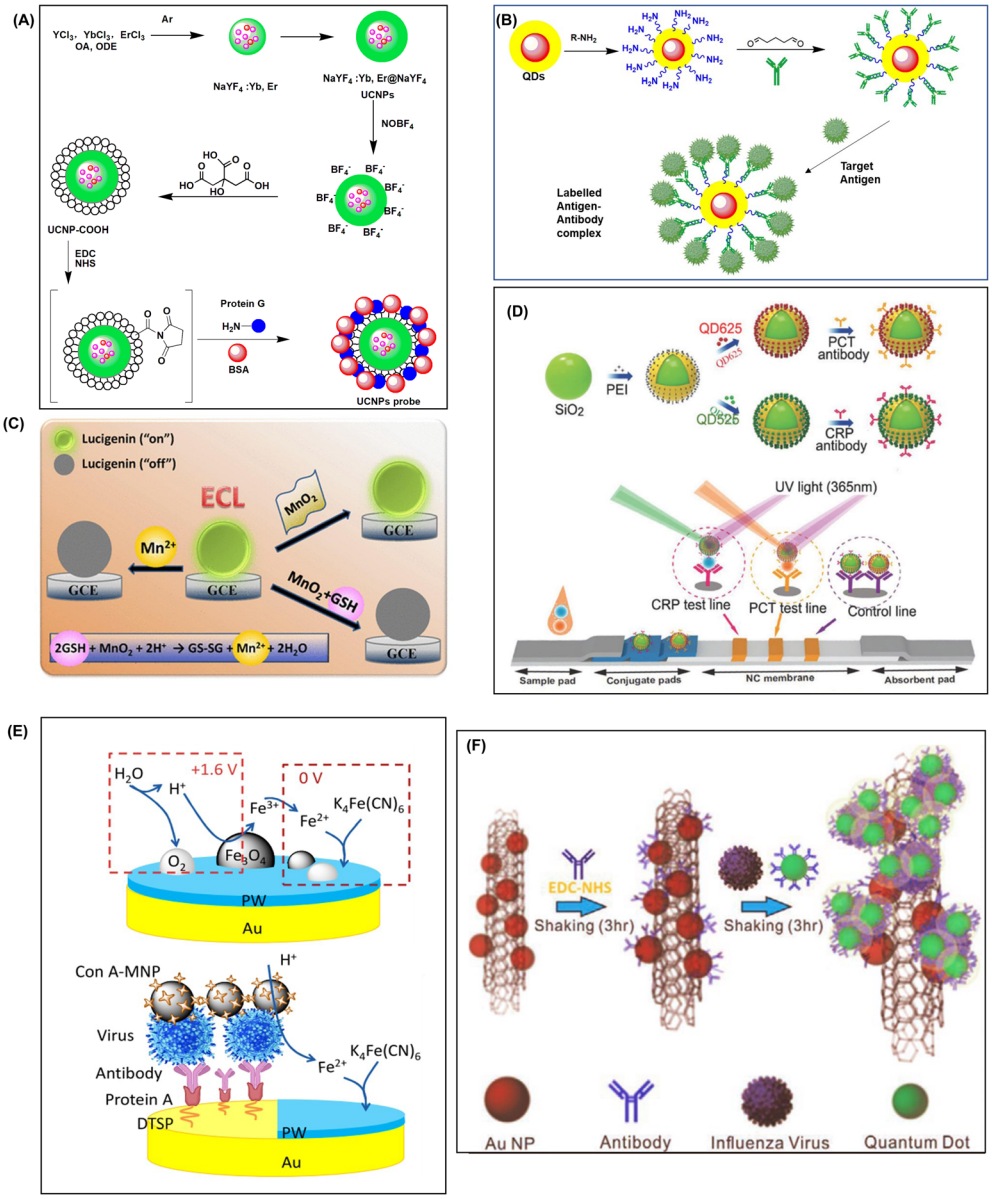

Fig. 6 Several types of nanoparticle and probe combinations. (A) Synthesis, surface modification, and bioconjugation of core–shell UCNPs through the EDC/NHS intermediate. Figure adapted from Hou *et al.*, *New J. Chem.*, 2020, **44**, 15498–15506. Copyright 2020, Royal Society of Chemistry. (B) The amino-modified QDs conjugated with antibodies through glutaraldehyde. (C) Schematic illustration of the measurement of GSH using lucigenin and MnO_2 nanosheets. Figure adapted from Gao *et al.*, *Anal. Chem.*, 2016, **88**, 7654–7659. Copyright 2016, American Chemical Society. (D) SiNPs bind with QDs nanobeads for the simultaneous detection of two sepsis biomarkers. Figure adapted from Yang *et al.*, *Microchim. Acta*, 2020, **187**, 570. Copyright 2020, Springer Nature. (E) Illustration of the electrochemical conversion (ECC) and ECC-based immuno-biosensor. Figure adapted from Zhang *et al.*, *Anal. Chem.*, 2017, **89**, 12145. Copyright 2017, American Chemical Society. (F) Development of influenza virus detection using AuNPs/CNTs. Figure reproduced with Lee, *Biosens. Bioelectron.*, 2015, **64**, 311. Copyright 2015, Elsevier.

absorption and reaction (SILAR) method, which involves self-assembly for the synthesis of a thin film on a solid support through the spontaneous deposition of nanoparticles without additional tagging or chemical modification for the early clinical diagnosis of HPV infection and the detection of malachite green-activated human carcinogenesis. Since silver and gold-modified nanomaterials lead to a strong surface plasmon resonance effect compared to other metals, they are widely used for surface-enhanced Raman scattering (SERS) implementation. Numerous researchers have focused on the bimetallic nanoparticle structure to increase the SERS enhancement factor and overcome silver oxidation.

SERS was discovered in the 1970s. It is a surface-sensitive resonance extension of standard Raman spectroscopy. The specimen/molecules of interest are placed in the vicinity or deposited on rough metals or semiconductor substrates, mainly on gold-, silver- or zinc-based nanoparticles. When excited specifically, interactions in the molecule–substrate system lead

to enhancement in the spectra.[76] The SERS-based platforms mainly utilize Raman shifts originating from molecular vibrational energy levels and distinguish structurally similar molecules according to the distinct vibrational spectra.[77] The combination of SERS tags and ICA strips is mostly based on Au/Ag SERS tags;[78] however, Au/Ag NPs are easily affected by environmental factors in complex samples. To overcome this problem, some strategies are adopted to improve the performance of SERS-based ICAs, for example, the optimization of particle size and shape to reduce nonspecific signals, enhance the stability of SERS tags for real sample detection, and enrich the analyte ability of SERS tags.[79] Methylene blue (MB)-adsorbed AuNPs coated with a silica shell were designed as an immunoassay platform for detecting SARS-CoV-2 spike (S) protein.[80] Dual-dye-loaded Ag-coated Fe_3O_4 MNPs (Fe_3O_4@Ag tags) were designed as magnetic SERS tags to detect respiratory viruses by Wang *et al.*[81] The work introduced Fe_3O_4@Ag SERS tags into the ICA strips, which can be used for real biological samples without sample pre-treatment steps. With the excellent conductivity of AgNPs, they are widely used as electrodes in electrochemical devices.

3.1.2 Gold nanoparticles (AuNPs). With unique optical, chemical, catalytic and electrochemical properties as compared to other nanomaterials, AuNPs are ideal signal amplification labels for immunoassays. They are easily prepared and the procedure only involves heating and stirring in common laboratories. The method was developed by Turkevich *et al.* in 1951 and was further modified by many other researchers.[82,83] The procedure is based on the chemical reduction of gold salts by reductants like citric acid, hydroxylamine hydrochloride, tannin, oxalic acid and sodium citrate. The particle size, shape, aggregation state and surface properties of AuNPs are tunable by adjusting the ratio of reactants or reductants,[84] and the sizes and shapes of AuNPs strongly influence their special properties and applications. AuNPs, possess unique LSPR characteristics with high molar extinction coefficients and exhibit aggregation or disaggregation-based chromogenic changes in the presence of the targeted analytes due to the variation in their size. AuNPs can produce a range of colors from wine red (smaller than 100 nm) to brown (larger particles), and these properties have been of interest for centuries.[85] Scientific reports on AuNPs (and other precious metal-based NPs) can be traced back to Michael Faraday.[86] The colloidal gold solution presents a red-to-blue (or purple) color change, which is also closely related to a dramatic LSPR shift, and provides a simple platform for colorimetric detection. AuNPs have a microenvironment compatible with biomolecules so their activity remains even after immobilization. Finally, the biocompatibility and biosafety of AuNPs are better than other inorganic materials[87] and their applications in immunoassay cover the majority of possible platforms. Several reviews have described the characteristics and advantages of AuNPs in detail;[88] herein, we only focus on specific applications of AuNPs in POCT ICAs.

AuNPs are dispersed in liquids to form stable colloidal gold, which is dependent on their shape, concentration, surface ligand, solution pH and ionic strength.[89] The common method uses the citrate reduction of chloroauric acid, resulting in AuNPs having negatively charged carboxyl groups with negative surface zeta potential. The negatively charged shells prevent aggregation and allow for the persistence of AuNPs. Once the carboxyl groups are deprotonated, they can inhibit nanoparticle aggregation by coulombic repulsion.[90] This probably maintains the zeta potential of the nanoparticle surface. A replacement of the trivalent citrate ions with monovalent mercaptan ions causes the destabilization of particles and leads to further aggregation and an increase in the size of the final nanoparticle aggregates. AuNPs are easily conjugated with biological ligands due to the strong affinity of sulfide to form stable M–S (metal–sulfides) bonds and amino functional groups without extra reagents to assist surface modification.[91] Thus, an electrical double layer appears on the surface of the gold particles.[92] Fig. 5A displays the chemical binding principle of immunogold formation. The first layer is known as the stern layer and is always positively charged. The second layer is known as the diffuse layer and is always negatively charged. The interaction forces between AuNPs and protein molecules are usually ionic bonds, dative covalent bonds, and hydrophobic bonds and so on. In addition, interlayer interactions, including hydrogen bonding, electrostatic attraction, and hydrophobic effects, may induce interparticle attraction without the citrates being displaced.[93] The external factors, solvent effects and substrate effects may disturb the formed structure and strongly affect the stability.

LSPR is produced at the interfaces of noble metal nanoparticles when they are stimulated by incident light. For certain nanostructures like AuNPs and AgNPs, the intensity and frequency of LSPR absorption are influenced by the surrounding environment and properties of the nanoparticles such as size, shape and surface coating.[94] The LSPR also produced a series of optical properties, which have been utilized for detecting proteins and nucleic acids. As shown in Fig. 5B, LSPR is produced at the interfaces of noble metal NPs when they are stimulated by incident light. The resonance can be achieved when the frequency of incident photons matches the natural frequency of surface electrons oscillating against their attraction to the positive nuclei.[95]

There have been several reports based on these nanoparticles. Hierarchical flower-like AuNPs, such as tipped flower-like, popcorn-like, and large-sized flower-like AuNPs have been prepared, and the tipped flower-like AuNPs integrated with ICAs showed high sensitivity for the determination of *E. coli* O157:H7 (Fig. 7A).[96] Positive detection signals are produced when the sensors encounter targets such as pathogens or pathogen by-products. The combination of novel AuNPs with ICAs enhanced the color intensity by more than two orders of magnitude as compared to the visual-antibody-macroarray.[97] These reports verify that the morphology of AuNPs greatly influences the sensitivity of ICAs. ICA platforms have also been used to detect nucleic acids. It has been reported that a DNA sensor for the African swine fever virus utilized AuNPs as the label.[98] As shown in Fig. 7B, cross-priming amplification (CPA) in combination with ICAs rapidly detected the African swine fever virus without cross-reactivity to other swine viruses with a minimum detection limit of 200 copies. MiRNA plays

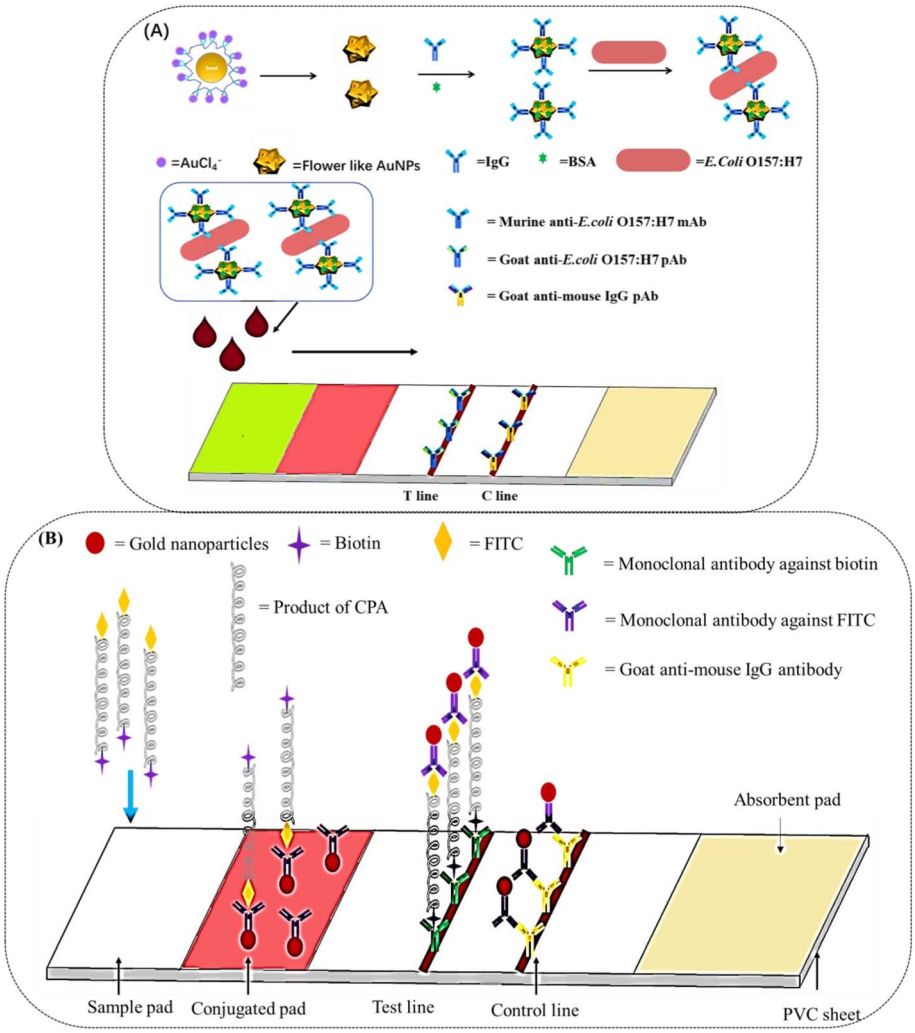

Fig. 7 (A) Surface functionalization of tipped flower-like AuNPs with antibody I (murine anti-*E. coli* O157:H7 mAb) and BSA; schematic illustration of the immunochromatographic detection of *E. coli* O157:H7. Figure adapted from Zhang *et al.*, *Langmuir*, 2015, **31**, 5537–5544. (B) Schematic diagram of the cross-priming amplification (CPA)-strip assay. Figure adapted from Gao *et al.*, *Sens. Actuators B Chem.*, 2018, **274**, 304–309.

important roles in biological processes; however, the traditional sandwich methods may not work well. Therefore, it was necessary to develop AuNPs-labeled ICTSs for miRNA detection.[99] The AuNPs conjugated with the thiol-DNA as the detection probe and the biotin-single strand DNA served as the capture probe, forming an avidin-biotin-AuNPs-sample complex. It provided a method for the detection of short oligonucleotides such as miRNA and siRNA. Stevens *et al.* designed a POC testing assay for detecting IgG antibodies against the Ebola virus in the serum of human survivors.[73] The platform was composed of ICTSs and a smartphone reader, enabling semi-quantitative detection and observation by the naked eye (Fig. 8), which would broaden the application scope of POCT.

3.1.3 Quantum dots (QDs). Colloidal semiconductor nanocrystals exhibit excellent optical properties, including absorbance and photoluminescence. In a narrow sense, QDs are typical semiconductor nanocrystals that are only a few nanometers in size and are prepared with core and core–shell configurations from two or more heavy metal elements,[100,101] such as II–VI (*e.g.*, CdTe and CdSe), and III–V (*e.g.*, InP). When high-energy electrons of QDs relax into holes, they emit electromagnetic radiation in the NIR or UV region of the electromagnetic spectrum. The sizes of QDs are of the same order as the exciton Bohr radius due to which electron bands in a QD exist in the form of discrete energy levels. Among the large number of fluorescence markers, QDs are ideal particles due to their unique optical properties. Modulating the chemical composition and particle size can adjust the fluorescence emission wavelength of QDs. The inclusion of additional elements in a QD can modify its intrinsic properties. The inert inorganic core coated with a shell to form core–shell QDs has good photochemical stability. QDs have a high fluorescence quantum yield (40–90%) and large molar extinction coefficient, up to 106 L (mol cm)$^{-1}$. QDs also have a lot of advantages, for example, long fluorescence lifetimes (up to 20–50 ns), high-resolution threshold, relatively narrow fluorescence emission, broad excitation range and excellent stability against

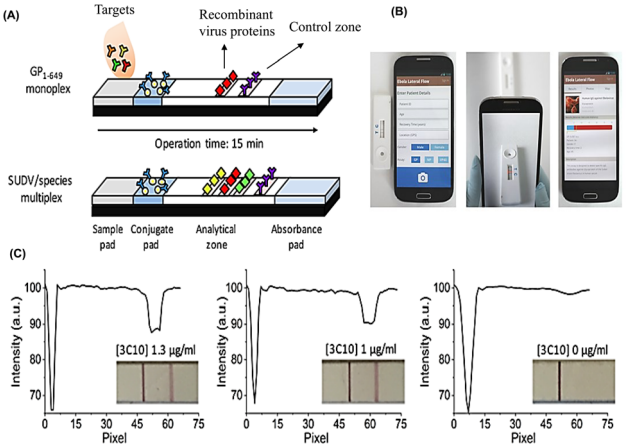

Fig. 8 Smartphone lateral flow point-of-care test for the Ebola virus IgG detection. (A) Lateral flow strip illustration. (B) Illustration of the smartphone application (app) interface login window to record patient details. (C) Assay strips and the corresponding raw intensity plots quantified by the smartphone app. Figure adapted from Brangel *et al.*, *ACS Nano*, 2018, **12**, 63–73. Copyright 2018, American Chemical Society.

photobleaching.[102,103] In recent decades, the development of QDs in many applications, ranging from molecular and cellular biology to molecular imaging and medical diagnostics, has attracted significant attention. Due to their advantages, QDs have been utilized in ICTSs as labels for detecting not only small molecules and nucleic acids but also proteins and even bacteria.[104,105]

Those QDs-labeled ICTS platforms have been widely used to detect proteins. Nanocrystal QDs have been prepared and used in ICA platforms to determine nitrated ceruloplasmin.[106] The biosensor displayed a rapid signal response for targets with a concentration of 1 ng mL^{-1} and exhibited a wide range with a LOD of 8 ng mL^{-1}. Although a large number of QDs have been reported for ICAs, safety is still an important factor. Traditionally, QDs have been mainly cadmium-based due to their excellent photostability, resistance to bleaching, wide excitation range in the ultraviolet spectrum, and narrow emissions. However, it is well known that some heavy metals, such as cadmium and chromium, have high toxicity. Taking the ASSURED criteria into consideration, cadmium-free NPs as labels are optimal. Accordingly, environment-friendly Cu:Zn–In–S/ZnS QDs have been reported for the ICA platform for the detection of tetanus antibodies.[107] In general, the application of ICAs in the detection of antibodies is relatively rare, and this research provides a reference for POC antibody determination.

It is known that the size of labels heavily influences the performance of ICSTs. However, QDs also have a small size; therefore, it is necessary to improve the size to optimize ICAs. Encapsulating numerous individual QDs into a polymer matrix to form QD nanobeads (QBs) can significantly increase the fluorescence intensity and environmental tolerance. This method enhanced the sensitivity and stability of fluorescent sensors. QBs were integrated with ICTSs to overcome the limitation of poor quantity and low sensitivity.[108] As reported, the QDs were encapsulated with modified poly(*tert*-butyl acrylate-*co*-ethyl acrylate-*co*-methacrylic acid) to obtain large QBs. The QBs-based ICTS platforms determined the prostate specific antigen (PSA) within 15 min and the LOD was enhanced. Pang *et al.* applied poly(styrene/acrylamide) copolymer nanospheres as carriers to embed CdSe/ZnS QDs to form fluorescent nanospheres that were greater than 200 nm in size,[109,129] which was 380-fold that of QDs. Fluorescent nanospheres were conjugated with a monoclonal antibody to detect CRP, which was 257-fold more sensitive than the colloidal gold-based ICA for CRP. In addition, two test lines were easily recognized under UV light. Mycotoxins are toxic by-products of metabolism produced in food contaminated by molds and are listed as a Group I carcinogen by the International Agency for Research in Cancer.[110] Aflatoxin B1 and ochratoxin A are easily generated in maize. Wang *et al.* synthesized highly fluorescent QBs by embedding CdSe/ZnS QDs with poly(methyl methacrylate) (PMMA) and poly(maleic anhydride-*alt*-1-octadecene) (PMAO).[111] After the surface was blocked, the labeled QBs were utilized as ICA signal amplification probes and showed dynamic linear detection of aflatoxin B1 in maize. As shown in Fig. 9A, Xiong *et al.* synthesized QBs with different sizes (58, 124, 255, 365, and 598 nm) and the results indicated that the optimal detection platform for ochratoxin A using competitive ICA was 124 nm QBs.[127] In addition, QBs have been developed for the simultaneous quantitative detection of neuron-specific enolase (NSF) and carcinoembryonic antigen (CEA).[112] In short, small-sized QBs or QDs had weaker fluorescence intensities than large-sized QBs; thus, the latter were more suitable in the ICA.

3.1.4 Magnetic nanoparticles (MNPs). A variety of iron compounds are superparamagnetic at particle sizes below 1000 nm, such as Fe_3O_4 and γ-Fe_2O_3. These MNPs can act as transducers and catalysts, as well as complexing agents for magnetic enrichment. It is much more sensitive than optical and electrochemical techniques to detect targets with magnetic sensors because interferents and non-specific molecules in complex biological media are nonmagnetic. As one of the most important NPs, magnetic nanoparticles (MNPs) have been exploited as candidates for POC testing platforms.[113] To the best of our knowledge, iron oxides are the most versatile magnetic NPs due to their excellent properties, such as high surface-to-volume ratio, easy fabrication, highly active surface, high chemical stability, excellent surface modification properties, and fast reaction kinetics.[114] Although these magnetic NPs can be directly used for biomodification, it is recommended that the magnetic beads are coated with a protective layer. In general, small magnetic particles ranging in size from 1 to 10 nm are paramagnetic and larger particles (μm) are ferromagnetic. Based on this, Fe_3O_4 magnetic NPs with super-paramagnetic properties can separate specific molecules from complex samples under a mild magnetic field to decrease the matrix interference of impurities in complex samples such as serum, urine and saliva. In addition, target enrichment can enhance the concentration and detection sensitivity, especially for the detection of multiple molecules. Besides, magnetic nanoparticles (MNPs) are also employed in electrochemistry modes. The electrochemical conversion (ECC) of magnetic

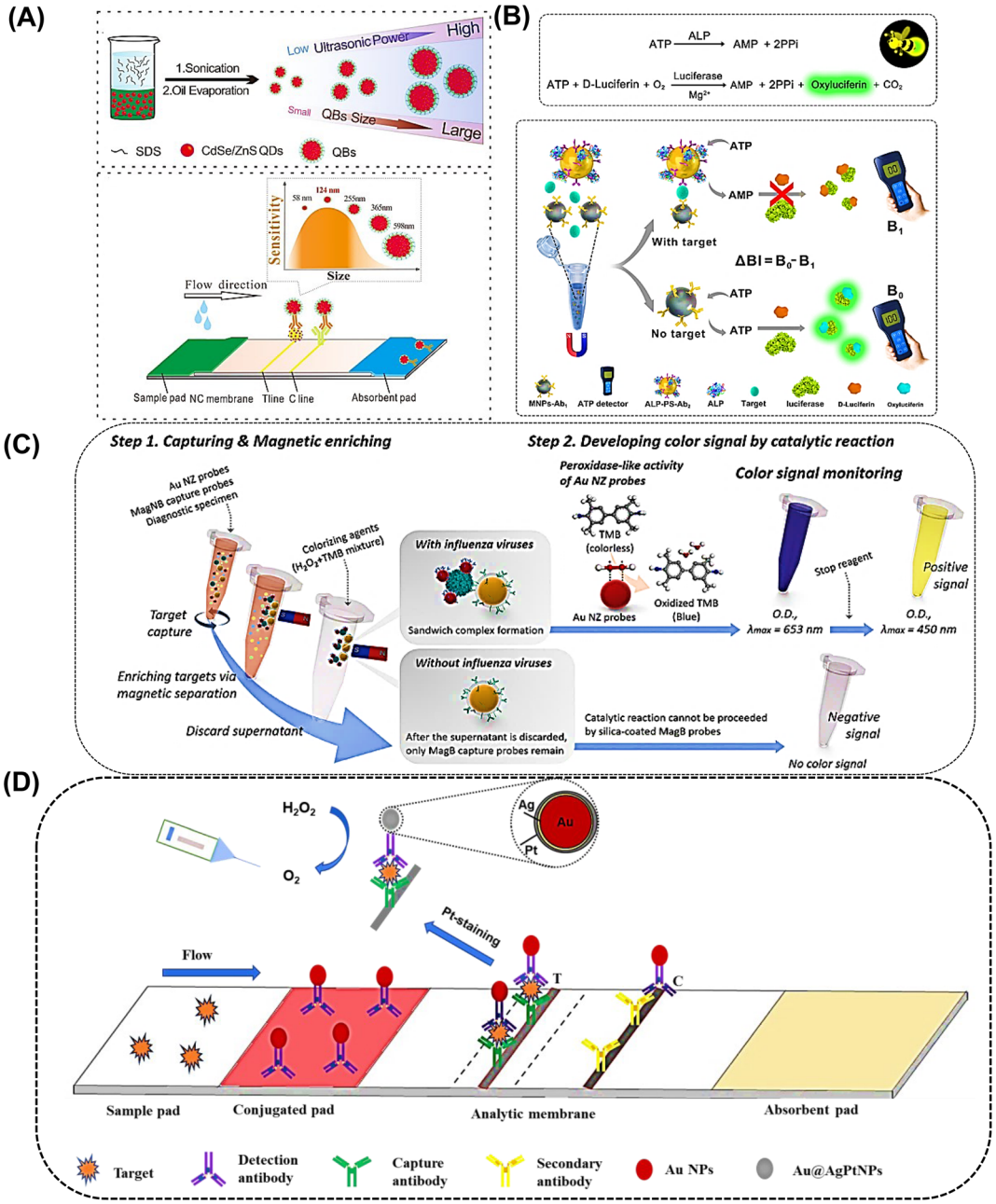

Fig. 9 (A) Schematic representation of the procedure for preparing different-sized QBs using the emulsion droplet solvent evaporation method. Figure adapted from Duan *et al.*, *Anal. Chem.*, 2017, **89**, 7062–7068. Copyright 2017, American Chemical Society. (B) Scheme of the ABS for the highly sensitive and quantitative detection of targets. Figure adapted from Chen *et al.*, *Anal. Chem.*, 2017, **89**, 5422–5427. Copyright 2017, American Chemical Society. (C) Working principle for the quantification of influenza viruses using the colorimetric diagnostics kit. Figure adapted from Oh *et al.*, *ACS Appl. Mater. Interfaces*, 2018, **10**, 12534–12543. Copyright 2018, American Chemical Society. (D) Working principle of colloidal gold test strips with Pt-staining for quantitative POC testing based on a pressure meter readout. Figure adapted from Huang *et al.*, *ACS Appl. Mater. Interfaces*, 2019, **11**, 1800–1806. Copyright 2019, American Chemical Society.

nanoparticles (MNPs) to electroactive prussian blue (PB) analogues was exploited for the biosensing of avian influenza virus H5N1.[115] Based on the ECC methods, a sandwich immunosensor was designed for the rapid detection of the avian influenza virus H5N1 using MNPs as self-sacrificial labels to produce PB for signal amplification. The ECC method involves a high-potential step to create strongly acidic conditions by splitting H_2O to release Fe^{3+} from the MNPs, and then a low-potential step leading to the reduction of coexisting $K_3Fe(CN)_6$ and Fe^{3+} to $K_4Fe(CN)_6$ and Fe^{2+}, respectively, which react to form PB analogues (Fig. 6E).

MNPs are often involved in target molecule carriers, signal generation and enhancement, separation, and purification steps in bioassays. This is due to their special combination with

more modestly-sized or same-sized molecular analytes, which follows a specific diagnostic approach with high sensitivity.[116] Gao *et al.* prepared controllable Fe_3O_4 particle aggregates by cross-linking PEG-coated Fe_3O_4 NPs bearing surface reactive carbonyl moieties with poly-L-lysine.[117] It is known that the aggregation of Fe_3O_4 NPs can generate a significant amplification effect, and the particle aggregates effectively increase the sensitivity of paraoxon methyl testing. Chang *et al.* designed a sensitive and dual-mode magnetic fluorescence ICTS based on PLGA@Fe_3O_4 super-paramagnetic nanosphere probes for two biomarkers of breast cancer.[118] Approximately 47 small-sized Fe_3O_4 NPs and approximately 2680 Cy5 molecules were encapsulated to form one super-paramagnetic nanosphere, which was integrated with ICA through sandwich immunoreactions. Moreover, the immunoprobe detected whole blood samples *via* magnetic separation and enabled quick naked-eye screening within 3 min. The probe simultaneously detected CEA and carbohydrate antigen (CA153) with high sensitivity.

Magnetic nanobeads are also jointly used with other nanoparticles, such as AuNPs and QDs. In the conventional assay, magnetic nanobeads are employed to separate and enrich targets from complex samples.[119] The magnetic nanobeads and AuNPs system has been utilized to detect malarial biomarkers.[120] The applied magnetic field separated the iron oxide NPs, as well as the AuNPs conjugated to the target. Therefore, large aggregates were efficiently separated from bulk serum, which resulted in an amplified signal without matrix interference. A double-enzyme-mediated bioluminescent sensor for adenosine triphosphate (ATP) determination based on immunomagnetic nanoparticles (MNPs) and polystyrene nanospheres (PSs) was reported.[121] As shown in Fig. 9B, a pair of ATP antibodies were conjugated with MNPs and PSs, respectively. Alkaline phosphatase (ALP) was also conjugated with polystyrene nanospheres and efficiently degraded ATP. In the presence of ATP, luciferase catalysed the oxidation of luciferin into oxidized oxyluciferin and produced bioluminescence, and the bioluminescence intensity was proportional to the amount of ATP. In another interesting example, Zhang *et al.* revealed multiple single nucleotide polymorphisms based on an ICA by combining an amplification refractory mutation system PCR with Fe_3O_4/Au NPs.[122] In the study, the magnetism of Fe_3O_4 was not applied to separate but to quantify DNA determination by detecting the magnetic signals at the test line. Of note, this is the first report utilizing the platform for the detection of multiple single nucleotide polymorphisms. In another study, the prepared Fe_3O_4/Au NPs were combined with monoclonal anti-hCG antibodies and used to detect human growth hormone in serum.[123]

Lee *et al.* reported an ultrasensitive colorimetric assay for influenza A virus detection known as magnetic nano(e)zyme-linked immunosorbent assay.[124] AuNPs and silica-shelled magnetic nanobeads were combined to enhance the sensitivity. The two types of NPs were conjugated with an antibody to further react with the virus, forming a sandwich pattern in the presence of the target virus (Fig. 9C). Magnetic nanobeads can realize simple target separation and gold nanozymes can realize signal amplification through enzyme-like activity, which enabled the sensitive identification of the influenza A virus at low detection limits both observed by the naked eye and detected by a microplate reader.

In addition, magnetic microbeads were designed for an electrochemical assay. Comerci *et al.* prepared a portable and robust electrochemical bio-probe based on magnetic microbeads for POC testing of diseases caused by parasitic protozoa, bacteria, and viruses.[125] The superparamagnetic microbeads were activated and conjugated with the corresponding antigens. Following the addition of samples and HRP-conjugated antibodies, the electrochemical signals were recorded on an 8-channel potentiator device.

3.1.5 Pt-group nanoparticles. The Pt-group metals, especially platinum, also play an important role in high catalytic activity and stability and are superior to natural enzymes.[126] These metals have been used to decorate other NPs to form a core–shell structure or form an electrode. The porous bimetallic Pt-NPs have provided excellent catalytic performance and have been considered promising nanomaterials in biomedical research for decades, owing to their high surface area, diverse composition and excellent electron conductivity.[127]

Catalytic activity is one of the most important properties of noble metals, which can greatly promote some chemical reactions. However, natural enzymes are fragile biomolecules and they easily lose catalytic activity even under normal assay conditions; therefore, they are not suitable for POC applications. Recently developed nanozymes based on inorganic nanomaterials have been attracting attention for noble metal NPs loaded with natural enzymes since they exhibit enzyme-like catalytic activities without denaturation, and thus can be stored and used under a wide range of pH and temperatures.[128] In particular, enzyme-catalysed biochemical reactions are important in humans and some POC diagnostic devices have been developed following this principle. Noble metals also play an important role in the catalysis process.[127] Thus, nanozymes can be easily produced on a large scale and exhibit increased catalytic activities due to their large surface area and specific catalytic potentials. This property has been utilized in diagnosis. Lin *et al.* reported that Pt–Au bimetal NPs were used for the detection of *Escherichia coli* O157:H7.[129] The NPs accumulated on the test line and simultaneously presented high catalytic activity towards 3,3′,5,5′-tetramethylbenzidine (TMB) and generated a specific blue color, which could be observed by the naked eye without an instrument. The reaction was fast and visualization of the blue color was observed in less than 1 min, and the detection limit was very low. The combination of Pt–Au bimetal NPs with the peroxidation catalysis reaction enhanced the signal by three orders of magnitude, which enabled the ultrasensitive detection of *Escherichia coli* O157:H7 and other bacteria.

Regarding the extension of the application of precious metals in POC assays, the catalytic activity of mesoporous Pt–Pd bimetal NPs was subsequently used to detect the p53 protein. The signal was generated through the strong peroxidase-like activity of Pt–Pd NPs, which displayed obvious catalysis of TMB and *o*-phenylenediamine (OPD). The color was observed within 10 min. Although the assay was less sensitive than the

advanced technology fiber light-coupled optofluidic waveguide immunosensor,[130] it was more sensitive than electrochemiluminescence detection.[131] However, the platform had strong stability in a wide pH range and temperature range. Another interesting example is that integrating the colloidal gold lateral flow assay and horseradish peroxidase (HRP) catalysis to achieve a dual-readout resulted in the chemiluminescent and ultrasensitive visual detection of disease biomarkers.[132]

Pt-group metals are also accompanied by other nanoparticles, and play a role in enhancing performance. Fe_3O_4 NPs have both magnetic properties and peroxidase-like properties. For example, Fe_3O_4–Pt/core–shell NPs were prepared and the catalytic activity could be further improved by incorporating Pt into the outer layers of the Fe_3O_4 NPs. Pt NPs were generated by the decoration of Pt on the Fe_3O_4 NPs surface by a heterogeneous nucleation and growth model. The new bioassay platform was proved to have a sensitivity that was two orders of magnitude higher than that of conventional Au NP-based ICA.[128] A pressure-based assay utilizing the strong catalytic property of PtNPs has been developed to provide quantitative detection. To overcome the long-term instability of PtNPs, a Pt-staining method was used to create platinum nanoshells on the surface of AuNPs. Utilizing this method, the original advantages of AuNPs were preserved and PtNPs were also introduced with catalytic activity as signal labels.[133] Another type of bioassay sensor has also been prepared. The core–shell Au@Pt nanoparticles were designed to catalyse the decomposition of H_2O_2 and release O_2, which can be employed to detect the carcinoembryonic antigen (CEA) and ractopamine.[134]

PtNPs have also been used to detect RNAs, which are significant biomarkers for cancer diagnosis and prognosis. For example, the PtNPs were prepared according to the sodium citrate and sodium borohydride ($NaBH_4$) reduction method. PtNPs and magnetic beads were used jointly to realize the qualitative detection of MicroRNA. Because of the catalytic decomposition of H_2O_2 by PtNPs, microRNA 21 can be detected by a POC assay through the strand displacement reaction.[135] Ge *et al.* reported a fluorescent/colorimetric dual-model biosensor based on the platinum nanocluster (PdNCs) for the detection of miRNAs. On the one hand, Pd NCs could catalyse a chromogenic reaction to obtain a qualitative result using the naked eye. On the other hand, the fluorescence quenching effect of graphitic carbon nitride on PdNCs was combined with nucleic acid cycle signal amplification to achieve precise results.[136]

Noble metals, especially Pd, Pt, Au, and their different alloys, also have excellent catalytic activity, and investigators have applied these properties to POC testing. This enables the signal magnitude to combine the ICA and catalytic activity of precious metals, enhancing the sensitivity and stability for either bacteria or proteins. This provides a new perspective for detecting biological molecules using POC immunoassays.

3.1.6 Upconversion nanoparticles (UCNPs). Optical ICAs have many advantages; however, they are limited by sensitivity and quantification. Therefore, to overcome the problem, large numbers of fluorescent nanoparticles have been exploited to replace traditional AuNPs. In recent decades, various fluorescent substances have been widely assembly into fluorescent ICTSs to address the deficiency of conventional colorimetric ICTSs. Generally speaking, for sandwich-like ICTS, a positive sample for the target analyte would involve both the test line and control line capturing the label-reporters, while a negative sample would involve the label-reporters only showing on the control line. The optical signal indicates the occurrence and strength of the immune reaction.

Upconversion nanoparticles (UCNPs), which are novel rare earth fluorescent particles, have emerged in recent years and have attracted great attention.[95] Since lanthanide ions have plenty of energy levels, the optical properties of UCNPs are tunable over both emission wavelength and lifetime and this improved the monochromatic color purity.[137] As shown in Fig. 10, under NIR excitation, UCNPs can generate the anti-Stokes process, where two or more low-energy photons are converted into high-energy output photons. UCNPs have many advantages over traditional NPs, such as high physical and chemical stability, minimal background autofluorescence, excellent light penetration depth, tunable multi-color sharp emission, and low cytotoxicity. All of these special properties make them suitable for bio-applications as optical reporters.[138,139]

In our previous work, rare earth salts were assembled into robust fluorescent UCNPs that were further functionalized with carboxyl and conjugated with specific proteins to sensitively detect the target antibody (Fig. 6A).[140] To enhance the fluorescence signal of UCNPs, Zhao *et al.* synthesized a series of $Na_{0.9}Li_xK_{0.1-x}YF_4$: Yb, Er UCNPs and found that when x was 0.07, the maximum intensities of both green and red emissions were observed.[141] The authors then conjugated the UCNPs with antibodies to accomplish the simultaneous dual-target detection of *Yersinia pestis* and *Burkholderia pseudomallei*. The assay achieved a sensitivity of 10^3 CFU per test without cross-interference between the two targets. For multiplex determination, Zhang *et al.* developed a multiplex lateral flow immunoassay to simultaneously detect four antibiotic residue families in milk.[142] As shown in Fig. 10F, the strips presented a green fluorescent line under 980 nm laser radiation, which showed high sensitivity and specificity. In Zhou's work,[143] the assay could tolerate samples with a wide pH range, high ionic strength, viscosity, and concentrations of bio-macromolecules. Moreover, the method exhibited high specificity for the three bacteria. Recently, Lee *et al.* developed a NIR-to-NIR UCNPs-based lateral flow immunoassay platform for the rapid and sensitive on-site detection of the avian influenza virus.[144] The authors prepared Ca^{2+}-doped UCNPs, which showed strong upconversion fluorescence emission centred at 800 nm upon excitation at 980 nm, making it possible to generate background-free fluorescence signals. Hence, these UCNPs have been used to detect targets in opaque stool samples without background interference. The LOD was more sensitive (10 times lower) than AuNPs whose absorption was masked by the brown background. A POC platform combining UCNPs and ICA has been developed for the quantification of myoglobin in clinical human blood samples.[145] The prepared core–shell $NaYF_4$:Yb, Er@$NaLuF_4$ nanoparticles showed stronger fluorescence

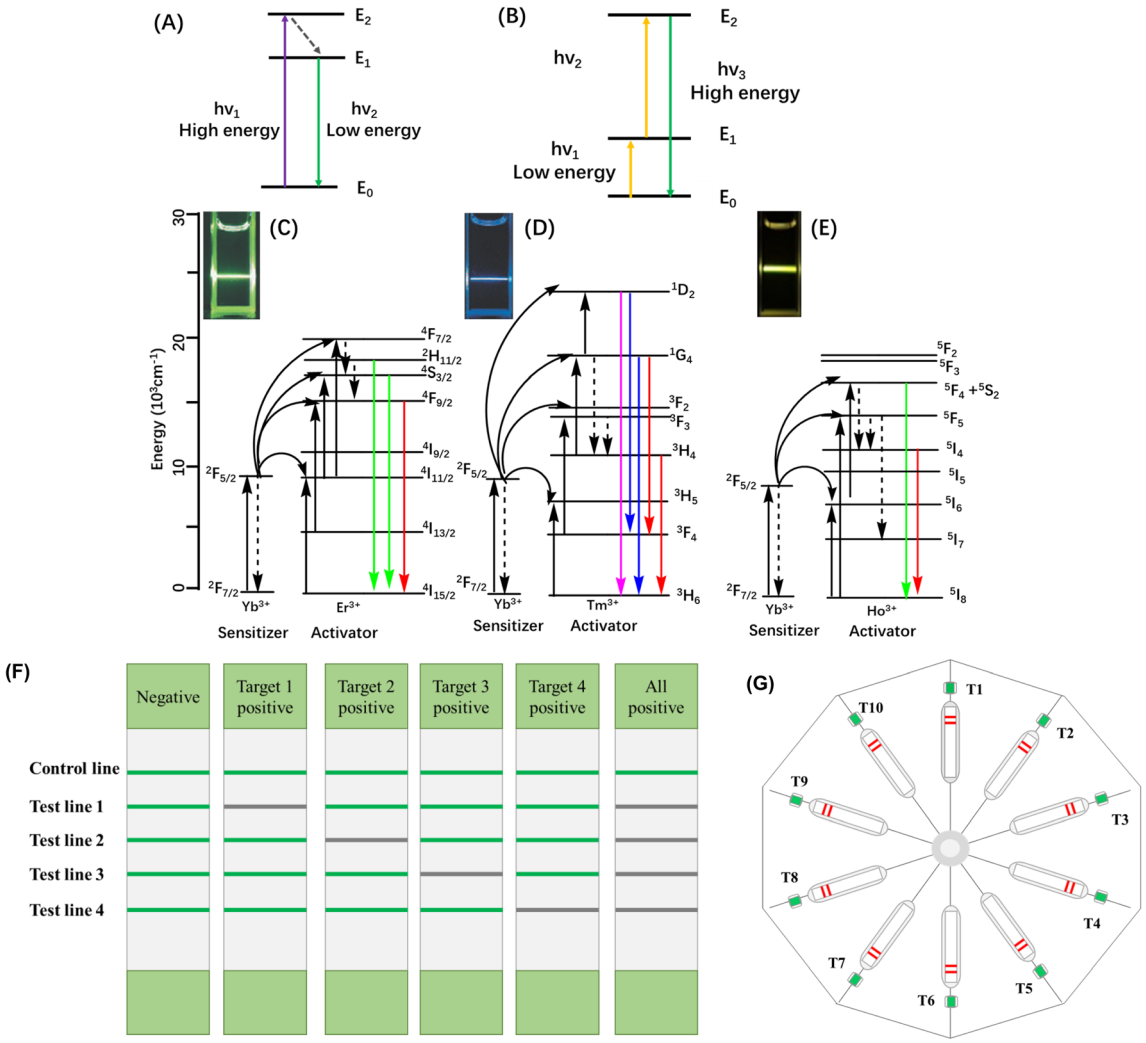

Fig. 10 Schematic principle of (A) conventional photoluminescence and (B) the mechanism of the upconversion luminescence process of the lanthanide UCNPs co-doped with (C) Yb^{3+} and Er^{3+}, (D) Yb^{3+} and Tm^{3+}, and (E) Yb^{3+} and Ho^{3+}. Figure adapted from Zhou *et al.*, *Chem. Rev.*, 2015, **115**, 10575–10636. (F) Lateral flow strips for the simultaneous detection of four different types of targets. Figure adapted from Chen *et al.*, *Biosens. Bioelectron.*, 2016, **79**, 430–434. (G) A sketch map of a multi-channel test disk. Figure adapted from Hong *et al.*, *J. Microbiol. Methods*, 2010, **83**, 133–140. There are 10 strip-holding channels arranged on the base in the central symmetry.

emission intensity than the parent core $NaYF_4$:Yb, Er. The UCNPs were coated with PAA and further combined with antibodies. A low LOD and a significant linear correlation with the clinically used Abbott chemiluminescence detection system (CLDS) were observed. So far, the platform of UCNPs and ICA has been employed to detect bacteria, viruses, antibiotic residues and biomarkers of diseases. In another study, Zhou *et al.* used up-converting phosphor technology combined with ICA for profiling antibodies against *Yersinia pestis*, which realized 10-channel determination (Fig. 10G).[146]

In other cases, the luminescence assay scheme consisted of UCNPs conjugated with an oligonucleotide probe and AuNPs linked with the target Ebola virus oligonucleotide. As a proof of concept, a homogeneous assay was fabricated and tested, yielding a detection limit at the picomolar level. Fluorescence resonance energy transfer (FRET) is ascribed to the spectral overlapping of upconversion luminescence and the absorption characteristics of AuNPs. The UCNPs and AuNPs were anchored on a nanoporous alumina (NAAO) membrane to form a heterogeneous assay.[147]

3.2 Nonmetal-based nanoparticles

3.2.1 Silicon nanoparticles (SiNPs). Silicon is the most common metalloid element used in nanomaterial-assisted target detection because it is cost-effective as well as non-toxic. Spherical silica nanoparticles (SiNPs) constitute the most popular shape of silicon-based nanoparticles. Mesoporous SiNPs with large pore channels and highly accessible inner surfaces have been used as nanocarriers for drugs, dyes and biomacromolecules. Therefore, some dyes or luminescent rare earth complexes have been doped into these particles to extend their application.

Typically, SiNPs were synthesized by a reverse microemulsion method and further functionalized with carboxyl or amino groups. Functionalized SiNPs were loaded with fluorescent molecules or nanoparticles to form fluorescent silica spheres. The fluorescent spheres were covalently linked with antibodies *via* carbodiimide cross-linking or improved periodate oxidation method, and then they were used for quantitatively detecting targets. For example, the SiNPs can load dyes, such as Reactive Violet 5, and are then encapsulated within a silica shell to form colored core–shell SiNPs.[57] Rare-earth complexes, such as Eu and Ru complexes, were coated in SiNPs for β-agonists detection.[148] QDs were also incorporated into silica spheres and further protected and functionalized with silica shells to enhance the robustness and sensitivity.[149] The fluorescent spheres were covalently linked with antibodies and were used for quantitative CRP detection. An on-site detection strategy based on the dual-color SiNPs@QDs realized the quantitative and simultaneous detection of C-reactive protein (CRP) and procalcitonin (PCT) in serum. The dual-color SiNPs@QDs nanotags, with monodispersity and excellent luminescence, were synthesized using the polyethyleneimine-mediated electrostatic adsorption of dense red CdSe/ZnS–COOH or green CdSe/ZnS–COOH QDs on the surface of SiNPs and were conjugated with anti-PCT and anti-CRP monoclonal antibodies as stable and fluorescence-enhanced QDs nanotags in the LFA system. The use of SiNPs@QDs with two different fluorescence signals caused the sensitivity and specificity of the multiplex LFA system (Fig. 6D).[150]

AuNPs were assembled with dendritic silica spheres through thiol-metal coordination to detect methamphetamine in urine samples.[151] SiNPs doped with organic dyes cost much less than Au, and they show satisfactory signal amplification. SiNPs are also suitable for loading a variety of substances ranging from organic dyes and small QDs to large enzymes. For example, pomegranate-shaped SiNPs (thickness: 5 nm) showed high uptake of QDs and they can be functionalized with antibodies for the detection of rabies lyssavirus.[152]

3.2.2 Polystyrene microspheres. Polystyrene microspheres, are polymer materials formed through the reaction of styrene, which have also been employed as carriers. Owing to their robustness and easy functionalization with carboxyl groups, they are widely used to load fluorescent materials. Lanthanides and their luminescent complexes (*e.g.*, Eu^{3+}, Tb^{3+}) provide reduced background signals and longer relaxation times with fluorescence in the microsecond to millisecond range.[153] Europium ions are also doped into polystyrene microspheres or silicon spheres, and then these particles are functionalized with carboxyl groups for conjugation with proteins. Eu-doped polystyrene microspheres have been applied in the detection of aflatoxins in feed,[154] silk fibroin in ancient silk,[155] clenbuterol in urine,[148] total thyroxine in serum,[156] polycyclic aromatic hydrocarbons in water,[157] antibodies in serum,[158] and even *E. coli.* O157:H7.[159]

In these fluorescent particles, SiNPs and polystyrene microspheres play the roles of vehicles for loading the fluorescent substance, which broadens the application of fluorescence materials and enhances the sensitivity and specificity of the ICA platform. However, the fluorescence assays still face the challenge of the fluorescence signal needing to be recorded by instruments. Recently, portable instruments have been made and they easily go from the laboratory to on-site detection. Moreover, the fluorescence signal is easily observed under UV light without the demand for sophisticated instruments. Because the signal in these strips is stable, the target can be real-time monitored qualitatively by the naked eye and further quantitatively detected using the instrument afterwards. In recent years, the instruments have been connected to mobile phone communication devices, which makes up for the shortcomings of some platforms that need instruments, moving closer to POC detection.

Some nanoparticles are not auto-fluorescent, such as AuNPs, PtNPs and graphene; however, they are also used in FICA by utilizing their properties to quench the fluorescence of other molecules or materials.[148] AuNPs have been jointly used with Cy5 to detect CEA with high sensitivity in 10 min.[160] On the one hand, the AuNPs aggregated at the test line can be recognized by the naked eye; on the other hand, fluorescence quenching can be calculated to quantitatively detect targets.

3.3 Carbon-based nanoparticles

Carbon exists abundantly on the earth and has therefore been widely applied in technological and scientific areas. Elemental carbon can exist as a variety of allotropes based on the hybridization of the carbon atom, *i.e.*, sp, sp^2, and sp^3.[19] Carbon-based nanomaterials have attracted wide attention over the last few decades, due to their unique advantages such as high surface-to-volume ratio, high electrical conductivity, chemical stability, and excellent biocompatibility.[161] Zero-dimensional (0D) nanomaterials such as carbon dots (CDs), graphene quantum dots (GQDs), and fullerene (C_{60}) are capable of undergoing dynamic and static quenching, electron transfer, energy transfer, and can be used as inner field-effect transistors (FET). One-dimensional (1D) carbon nanomaterials are based on carbon nanotubes (CNTs), including single-walled carbon nanotubes (SWCNTs) and multi-walled carbon nanotubes (MWCNTs). Two-dimensional (2D) carbon allotropes include graphene and its derivatives, such as graphene oxide (GO) and reduced graphene oxide (rGO).

3.3.1 0D carbon allotropes. In recent years, 0D carbon allotropes have been developed for use in detection sensors due to their electrical and optical features, such as fluorescence, chemiluminescence, photoluminescence (PL), and electrochemiluminescence. These nanoparticles can be conveniently and cost-effectively synthesized, composited and functionalized. Carbon dots have been demonstrated to be biocompatible and environmentally-friendly. With strong quantum yields, CDs have shown a longer lifespan and sensitivity two orders of magnitude higher as compared to gold colloid.[54] SiNPs can be used to prevent the fluorescence quenching of CDs at high concentrations, resulting in an increase in monodispersity and greater quantum yields. In addition, fluorescent CDs have been immobilized on dendritic SiNPs, and employed as a colloid for the colorimetric POCT of ZikV.[162]

3.3.2 1D carbon allotropes. Carbon nanotubes are composed of single or multiple graphene sheets that are wrapped into cylindrical tubes with different diameters. Both single-walled carbon nanotubes and multi-walled carbon nanotubes, have been used to modify electrodes and are further applied in the selective detection of dopamine, human serum albumin, epinephrine, toxins and cancer biomarkers.[163] Common coupling chemistries have been explored to conjugate CNTs with receptors such as cysteamine, ethyl(-dimethylaminopropyl)carbodiimide (EDC) with *N*-hydroxysuccinimide (NHS), (3-aminopropyl)triethoxysilane (APTES), and glutaraldehyde. CNTs are versatile nanomaterials and chemical functionalization can greatly alter their sensing capabilities. Carbonylated CNTs can couple with viruses or proteins to form specific sensors. These CNTs exhibit excellent electrochemical stability and induce greater electron transfer through amide bonds with amino-containing moieties. Aminated CNTs in immunosensors amplify the charge transfer and provide a stable platform for antigen immobilization.

CNTs-based biosensors possess high selectivity and sensitivity due to their high surface area; they are also useful because of their ease of functionalization. For instance, a modified electrode was assembled with multi-walled carbon nanotubes (MWNT), polypyrrole nanowires (PPNWs) and AuNPs to enhance selectivity and sensitivity. This electrode provided a porous structure with a large effective surface area, high electrocatalytic activity and electronic conductivity. Therefore, the amount of DNA aptamer immobilized on the electrode was increased while the accessibility of the detection target was maintained.[164]

Another strategy for tuning the characteristics of CNTs includes decoration with metallic nanoparticles. AuNPs have been interspersed on MWCNTs to introduce peroxidase-like activity. The coexistence of nanoparticles in CNT nanocomposites offers four key benefits as follows: (1) a stronger electrochemical response due to synergistic electronic interactions; (2) receptor conjugation is encouraged *via* H bonding, π–π interactions and electrostatic forces; (3) the increased surface area enhances analyte adsorption; (4) improved biocompatibility.[165] AuNPs-decorated CNTs were developed for the detection of the influenza virus. Specific antibodies (Abs) against the influenza virus were conjugated on the surface of AuNPs-CNTs and QDs, which had photoluminescence intensity that varied as a function of the virus concentration and a detection limit of 0.1 pg mL^{-1} for all three types of influenza virus examined (Fig. 6F).[166]

3.3.3 2D carbon allotropes. Graphene has a two-dimensional (2D) carbon crystal structure and remarkable properties, such as fast electron transport, high chemical stability and strong mechanical strength, due to the unique structure of the electronic bands. The morphology of carbon-based nanomaterials has a great influence on their function and application. Graphene and graphene oxide are typical two-dimensional materials that are also utilized in electrochemical assays.[167] Cysteine-modified reduced graphene oxide (rGOs) was coated with gold nanoparticles, which were further functionalized with specific antibodies *via* EDC-NHS chemistry.[168] The covalent binding of S–Au between Cys-rGO and gold nanoparticles makes it easier to adjust the working electrode. The abundant functional groups, high surface area and biocompatible of mesoporous Cys-rGO hydrogel make it possible to load large numbers of antibodies, resulting in high sensitivity, selectivity and more kinetic binding.

The field-effect transistor (FET)-based biosensing device has been used for detecting SARS-CoV-2 in clinical samples.[169] In the assay, graphene is the sensing material and the SARS-CoV-2 spike antibody is conjugated on the graphene sheet *via* 1-pyrene-butyric acid *N*-hydroxysuccinimide ester, which is an interfacing molecule as a probe linker. The FET of rGO was developed to rapidly and sensitively detect the pathogenic rotavirus. Single-layered and large-sized GO sheets, greater than 50 μm, were prepared by a modified Hummers' method, and through the photolithography and reduction process. After integration into a polydimethylsiloxane microfluidic channel, specific rotavirus antibodies were covalently anchored to the graphene surface on which 1-pyrenebutyric acid *N*-hydroxysuccinimide ester was pre-adsorbed through π–π interactions.[170] The carboxyl-modified graphene materials are easily conjugated with biomolecules through NHS activation.

The potentiometric sensor contains an amplified signal composed of a metal oxide semiconductor field-effect transistor and a signal generator containing separate gold-coated chips. The immunosensor was highly sensitive and selective for anti-gE in real samples. To maximize the advantages of electrochemical sensing, carbon materials and noble metal nanoparticles were combined to enhance the performance. rGO/Ni/PtNPs micromotors and an Au electrode were integrated to rapidly and accurately detect C-reactive protein (CRP).[171] The AuNP/rGO nanocomposite was prepared *in situ* to increase electrocatalytic performance. The sensor was used to detect endometriosis marker CA125 in the blood of endometriosis patients with a dynamic linear range and a low limit of detection.[172]

3.4 Organic nanoparticles

Covalent organic frameworks (COFs) and metal–organic frameworks (MOFs) are the two main organic framework nanoparticles. They exhibit extraordinary thermal stability and low densities. However, due to the absence of high-energy electrons, COFs have only been used once for virus recognition. In contrast, MOFs are the most quotidian of organic nanomaterials that are in use for virus or protein detection. Their surface-to-volume ratio is high and their pore size can be easily altered. MOFs are fundamentally coordination polymers in which the organic component links metal ions to generate intricate architectures.[173] MOFs readily undergo π–π stacking interactions with viral DNA in addition to hydrogen bonds and electrostatic interactions. These interactions have also been confirmed using computational simulations and they enable the picomolar detection of Ebola RNA.[174] Dendrimers are polymeric nanoparticles consisting of three hierarchical constituents: (i) a medial core; (ii) intermediary layers of repeating units termed as ''generations''; (iii) an exterior layer of functional

groups bound to the outermost generation of the intermediary layers. They possess a globular shape with multiple functionalities on the surface, which are useful for biomolecular immobilization. In recent years, the scope of dendrimers in target detection has expanded beyond their role as immobilization platforms and nanomaterial carriers. Dendrimer nanocomposites possess interesting features such as bright fluorescence, sensitivity in complex media, and high reproducibility. The cornucopian tertiary amine groups in polyamidoamine (PAMAM) introduce water solubility and chemical stability in addition to enhancing the capacity for loading QDs.[175]

Molecularly imprinted polymeric nanoparticles (MIP-NPs) are nanoparticles that are fabricated as a result of the polymerization of one or more functional monomers in the presence of a template molecule. The template molecules are subsequently removed to reveal high-affinity target-specific nanocavities that are cost-effective and durable substitutes for antibodies.[176] MIP-NPs are becoming potential nanomaterials for antigen sensing because of their simple synthesis and their recalcitrance to extreme environments.

3.5 Other novel metal composite materials

Recently, researchers have focused on enhancing POCT sensitivity and specificity by optimizing the sensing platform from different perspectives. Therefore, some novel metal-related POCT platforms have been developed. Novel metal-related materials also jointly combine two or more NPs to optimize the platform by employing the functions of different NPs. This strategy is becoming a trend for the development of novel and practical immunosensors.

QDs are well-known fluorescent semiconductor materials. Manganese dioxide (MnO_2) nanosheets are redox-active layered transition-metal dioxide nanomaterials and have been used in biosensing and biomedicine due to their large surface area, intense and broad optical absorption, strong oxidation ability, catalytic activity, and robust mechanical properties.[177] QDs and manganese dioxide (MnO_2) nanosheet nanocomposites have been developed for the detection of glutathione.[178] Biotin-functionalized QDs were mixed with MnO_2 nanosheet solution under mechanical stirring to produce the biotin-QDs-MnO_2 nanocomposite owing to electrostatic interactions. GSH was oxidized to glutathione disulfide (GSSG) by MnO_2, and MnO_2 was reduced to Mn^{2+}, resulting in the decomposition of the MnO_2 nanosheets and the release of fluorescent QDs. MnO_2 nanomaterials have high peroxidase-, oxidase-, and catalase-like activities due to the presence of lattice oxygen defects that were recently found to be capable of catalyzing the reactions of organic substrates [(TMB), *o*-phenylenediamine (OPD), and diazoaminobenzene (DAB)] in the absence of H_2O_2 to produce a color reaction. MnO_2 nanosheets possess oxidase-like activity that can catalyze the oxidation of TMB. Meanwhile, the existence of GSH can cause the reduction of oxidized TMB, which will generate a visual color change. Mn^{2+} can inhibit the ECL of lucigenin. When MnO_2 nanosheets were reduced to Mn^{2+} by GSH, an obvious inhibition of the ECL of lucigenin was observed. The ECL inhibition efficiencies gradually increased when the concentrations of GSH increased (Fig. 6C).[179]

It has been demonstrated that noble metal NPs have capacitive ability, which can trap electrons and discharge them to suitable electron acceptors.[180] Therefore, these particles are easily conjugated with other nanomaterials, such as TiO_2, silica, graphene and other carbon materials to form metal compositions or core–shell structures. Wan *et al.* designed a sandwich-type immunosensor with Au–TiO_2, glucose oxidase (GOD), and anti-apolipoprotein E nanobodies.[181] The Au–TiO_2 was the amplifier to increase the loading capacity, GOD was employed to catalyse the glucose to produce H_2O_2, and anti-apolipoprotein E nanobodies were the detection antibodies. The indium tin oxide (ITO)-based POCT can detect apolipoprotein E and reveal similar results without the complicated analytical device preparation. An optical microfiber was used for POCT after surface functionalization. Huang *et al.* designed an optical microfiber sensor functionalized with a polystyrene@gold nanosphere interface to detect the carcinoembryonic antigen (CEA)-related cell adhesion molecule 5.[182] With the synergistic sensitization effect coupled with surface area enlargement and electromagnetic enhancement of the interface, the sensitivity was also enhanced by about 6 orders of magnitude as compared to current methods.

The resonance Raman scattering (RRS) of inorganic semiconductor nanomaterials as fingerprint signals to label biomolecules can resist environmental interference. ZnO is a third-generation semiconductor and is environmentally friendly. Nanostructures such as nanorods, nanobelts, nanodisks, nanosheets, nanopores, and radial nanowires were synthesized from these semiconductors.[183] To overcome the poor water solubility and instability of ZnO, it was coated with SiO_2 to form nanocomposites. The nanocomposites combined the RRS fingerprint signal and unique infrared (IR) fingerprint absorption of SiO_2, resulting in a dual-mode immunosensing platform for CEA detection.[184] The platform provided a novel method for the development of the POC immunoassay.

These different systems have also been integrated to form new platforms to optimize these methods. Based on one-dimensional ICA, Linnes *et al.* designed two-dimensional paper networks to perform ELISAs for protein detection.[185] AuNPs conjugated with both streptavidin and HRP as the medium simplified the process and enhanced the sensitivity. Xu *et al.* proposed an enhanced centrifugation-assisted lateral flow immunoassay to rapidly detect protein biomarkers in whole blood, which had a higher sensitivity than common ICA. The nitrocellulose membrane loaded the captured antibody and anti-mouse IgG was inserted into a centrifugal disc, and AuNPs and catalyzed DAB were utilized to simplify the signal.[186]

The heavy metals family is large and diverse, not only due to the number of elements but also due to their wide applications. QDs, MNPs and Pt-group metals are the most important particles of these metals. QDs have excellent fluorescence properties and stability and their size is easy to control; hence, they are widely used in diagnosis. MNPs are also used to separate molecules in an external magnetic field, which can aggregate targets and reduce background interference. Pt-group metals,

Table 3 List of commercial POCT diagnostic tests[a]

Product	Manufacturer	Time	Targets/samples	Technology	Approved	Country of origin
EPOC	Siemens	1 min	Whole blood	Electrochemical	FDA	Canada
ePlex	Gen Mark	—	Nucleic acid	Electrochemical	CE and FDA	USA
BinaxNOW COVID-19 Ag card	Abbott Diagnostics Scarborough, Inc	15 min	Antigen	LFA	U.S. FDA EUA	USA
WANTAI SARS-CoV-2Ab rapid test	Beijing Wantai Biological Pharmacy Enterprise Co., Ltd	15 min	Antibody in serum	LFA-colloidal gold	FDA	China
Sofia SARS antigen FIA	Quidel Corporation	15 min	Antigen	FLA-fluorescence	U.S. FDA EUA	USA
Novel coronavirus 2019-nCoV antibody test	Beijing Hot View Biotechnology Co., Ltd	15 min	IgM and IgG antibody	FLA-UCNPs	NMPA	China
LumieaDx SARS-CoV-2 Ag test	LumiraDx UK Ltd.	12 min	Antigen	Microfluidic	U.S. FDA EUA	U.K.
Coronavirus (COVID-19) IgG/IgM rapid test	Voxtur Bio Ltd., Surat (Gujarat)	—	Antibody	LFA	ICMR	India
STANDARD Q COVID-19 Ag	SD biosensor	—	Antigen	LFA	ICMR	South Korea/ India
CareStart COVID-19 IgM/IgG	Access Bio, Inc.	—	Antibody	LFA	FDA	USA
Tell Me fast novel coronavirus (COVID-19) IgG/IgM antibody test	Biocan diagnostics Inc.	—	Antibody	LFA	FDA	Canada
Sienna-clarity COVIBLOCK COVID-19 IgG/IgM rapid test cassette	Salofa Oy	—	Antibody	LFA	FDA	Finland
SGTi-flex COVID-19 IgG	Sugentech, Inc.	—	Antibody	LFA	FDA	Korea
ScheBo SARS-CoV-2 quick	ScheBo Biotech AG	—	Antibody	LFA	U.S. FDA EUA	Germany
SARS-CoV-2 antigen rapid test cassette (Swab)	Spring Healthcare Services AG	—	Antigen	LFA	U.S. FDA EUA	Switzerland
Snap® Parvo	IDEXX (Westbrook, USA)	8 min	Faeces	ELISA	U.S. FDA EUA	Germany
Glucometer	Omron	<5 min	Glucose in blood	Electrochemical	NMPA	China
Diagnostic kit for hCG	Runbio Biotech. Co., Ltd.	<5 min	hCG in urine	LFA	—	China
STANDARD F	SD BIOSENSOR	—	Antigens from hepatitis, blood-borne, chronic disease, inflammation, cardiovascular, hormones	LFA-europium beads	CE	Korea

[a] National Medical Product Administration, CN (NMPA); Indian Council of Medical Research Department of Health Research, Ministry of Health and Family Welfare, Government of India (ICMR); Food and Drug Administration, U.S.A. (FDA); emergency use authorization (EUA), Conformite Europeene (CE), Therapeutic Goods Administration (TGA).

such as AuNPs, AgNPs and PtNPs, have been widely used in the diagnostic field, owing to their excellent redox activity and optical performances. These NPs have been modified by other molecules or materials and have been applied in different platforms according to the detection mechanism. To improve the detection properties of these NPs, different nanoparticles have been integrated to optimize the immunosensors. For instance, the most conventional labels, AuNPs, have been designed to combine with QDs, magnetic particles, fluorescent NPs, UCNPs and so on. These immunosensors combined with ICA have been developed from one test line to two or three test lines, which enables the analysis of different analytes at the same time and realizes the multi-parametric analysis of the system. Moreover, a lateral flow immunosensor has been incorporated into other technology, for example, a personal glucose meter (PGM), to detect disease biomarkers such as PSA.[187] Therefore, these particles are utilized in POC assays and obtain excellent effects.

4 Conclusions and perspectives

Nanotechnology has brought a significant revolution to the existing biosensing technologies. This review elucidates the significant relevance of different platforms and nanoparticles to

achieve excellent performance. To improve the effects of these immunosensors, different labels, sample treatments and signal readout modes have been employed.

A thorough understanding of nanomaterial interactions in these POCT systems could help us to accelerate the development of analyte detection platforms with high veracity. Although the POC assay utilizing biosensors has made great progress, there are still some deficiencies to be resolved in real applications; for instance, some platforms are only used in buffers and not in real samples, and signal readout requires special equipment. Some devices mainly focus on the sensitivity and accuracy of the sensors. Only a few have reached the preclinical phase to test real samples; their simplicity is also neglected. Sophisticated operators and complicated approaches are also required for lots of platforms. Besides, many analysis targets exist in complex matrices and they are difficult to recognize. The diagnostic results are easily interfered with and, therefore, it is important to avoid false-positive results. Much work is still required to realize clinical applications that can be operated by different people in different environments. The reproducibility of these platforms has to be demonstrated using real samples before they are formally used in clinical diagnosis. Current immunosensors are prepared under optimal conditions in a laboratory and some bench researchers may ignore the clinical demand; therefore, how to realize real clinical translation and mass production with good reproducibility is still a challenge. It is critical to minimize the variation in different batches to prepare reproducible immunosensors. Only a combination of scientists, clinicians and engineers can develop practical platforms for applications from the laboratory to the clinical setting.

Numerous POCT devices are available in the market, including glucose monitoring, pregnancy and infertility testing, infectious disease testing, cholesterol testing and cardiac markers (Table 3).[188–190] Blood glucose monitoring once had the largest POCT market share, followed by pregnancy testing and critical care testing for various diseases and genetic disorders.[191] Table 2 compiles some of these systems available today for *in vitro* diagnosis (IVD). As a whole, samples used in these POCT assays are non-invasive or minimally invasive accessible biological fluids, such as blood, sweat, tears, saliva, and interstitial fluids (ISF). Most commercial POCT assays are based on LFA to detect antigens or antibodies. As introduced in detail earlier, the LFA platforms also contain three elements, visualized nanoparticles to generate the signal, antigen/antibody at the test line and control line. The reason the assays are popular all over the world is that the ASSURED criteria are highly available for these platforms. The second widely used POCT assay is based on electrochemistry. The glucometer is the typical representative. The detection mechanism has been introduced above. Compared with the LFAs, the glucometer is relatively complicated and a small device is indispensable. Such devices are used by those who have special requirements to monitor physical health indicators. ELISA is widely used in the laboratory. Other assays, such as microfluidic assay and microarray, are also based on LFA or electrochemistry more or less. These three assays are high-throughput, there is no advantage for them to be used by individuals.

In the past three years, commercial POCT products have been used to detect coronavirus, including LFA, chemiluminescence, microfluidic assay, and other assays.[192] Although some products have been authorized by Food & Drug Administration Emergency Use Authorizations (FDA EUA), Conformite Europeenne (CE) or Therapeutic Goods Administration (TGA), there is also a big gap in following the ASSURED rule. For instance, the price of POCT for the detection of canine parvovirus in Germany ranges from €4 to €14.[193] In China, the price of ICTSs is even as low as ¥2.0, as for pregnancy test strips, and other strips for metal ions; the price of blood glucose meter test strips is also less than ¥10.0. Therefore, POCT products are affordable.

Taking commercial POCT products for Covid-19 as an example, the positive/negative agreement was over 90%, even 95% with a few exceptions,[192] which means the sensitivity and specificity are acceptable. Most of the assays are finished within 20 minutes and can be stored at 2 °C to 8 °C for at least six months, yielding relatively robust and rapid results. As we know, the results of some LFAs are read by the naked eye, according to the color of colloidal gold, which is equipment-free, simple to perform and easy to carry; however, especially for some novel and sensitive assays, machines are indispensable and, therefore, they are far from the U, R, E, D of the ASSURED criteria; for example, the products from Luminex Corporation and Bio Check, Inc. It is difficult to balance the sensitivity with an equipment-free setup. Smartphones and wearable diagnostics make it possible for some sophisticated instruments to be used in POCT assays. Smartphones serve as minicomputers for sensitive and specific data quantification with built-in sensors, high-resolution cameras, rapid wireless connectivity, the ability to use many software and apps and hence, alone, can be integrated as sensors and detectors in mobile POCT. The wearables can be physical sensors to detect emotions, motion, heart rate, body temperature or biochemical sensor-based samples from the skin, eyes or mouth with minimal invasion. This type of testing is especially important to people suffering from critical illness because they can monitor their health intermittently without going to the hospital or needing professional training.[188]

Future perspectives for nanoparticle-regulated biosensors for POCT assay are related to the developments of both sensing methodologies and signal readout modes, which will assist in the miniaturization of POCT devices for ASSURED criteria. The integration of different types of nanomaterials to generate multifunctional nanocomposites will not only positively influence the sensitivity but also improve the signal-to-noise ratio and make the platform suitable for commercialization. Improving the stability of the immunosensors is key to ensuring their practicality. Advanced detection technologies and material development play a major role in modern biosensing and consistently provide significant improvements toward robust, sensitive, and versatile platforms for early detection.

Author contributions

Conceptualization, and writing—original draft preparation, F. H.; writing—review and editing, S. A., Y. T. and X. L.; supervision and funding acquisition, S. S. and H. C. All authors have read and agreed to the published version of the manuscript.

Conflicts of interest

There is no conflict of interest about this article.

Acknowledgements

This work was supported by the National Natural Science Foundation of China (32072859, 32072847, 32002272), the National Key R&D Program of China (2021YFD1800300), Science and Technology Major Project of Gansu Province (21ZD3NA001), and Science and Technology Talents and Platform Program (202205AF150007).

References

1 N. Young, M. Taegtmeyer, G. Aol, G. M. Bigogo, P. A. Phillips-Howard, J. Hill, K. F. Laserson, F. Ter Kuile and M. Desai, *PLoS One*, 2018, **13**, e0198784.
2 D. Quesada-Gonzalez and A. Merkoci, *Chem. Soc. Rev.*, 2018, **47**, 4697–4709.
3 V. Gubala, L. F. Harris, A. J. Ricco, M. X. Tan and D. E. Williams, *Anal. Chem.*, 2012, **84**, 487–515.
4 C. D. Chin, V. Linder and S. K. Sia, *Lab Chip*, 2012, **12**, 2118–2134.
5 S. Nayak, N. R. Blumenfeld, T. Laksanasopin and S. K. Sia, *Anal. Chem.*, 2017, **89**, 102–123.
6 E. Noviana, C. P. McCord, K. M. Clark, I. Jang and C. S. Henry, *Lab Chip*, 2020, **20**, 9–34.
7 Z. Zhang, P. Ma, R. Ahmed, J. Wang, D. Akin, F. Soto, B. F. Liu, P. Li and U. Demirci, *Adv. Mater.*, 2022, **34**, e2103646.
8 R. W. Peeling, K. K. Holmes, D. Mabey and A. Ronald, *Sex. Transm. Infect.*, 2006, **82**, 1–6.
9 O. Pashchenko, T. Shelby, T. Banerjee and S. Santra, *ACS Infect. Dis.*, 2018, **4**, 1162–1178.
10 A. N. Baker, G. W. Hawker-Bond, P. G. Georgiou, S. Dedola, R. A. Field and M. I. Gibson, *Chem. Soc. Rev.*, 2022, **51**, 7238–7259.
11 L. Tang and J. Li, *ACS Sens.*, 2017, **2**, 857–875.
12 Y. Wang, R. Hu, G. Lin, I. Roy and K. T. Yong, *ACS Appl. Mater. Interfaces*, 2013, **5**, 2786–2799.
13 B. V. Chikkaveeraiah, A. A. Bhirde, N. Y. Morgan, H. S. Eden and X. Chen, *ACS Nano*, 2012, **6**, 6546–6561.
14 Y. L. Xianyu, Q. L. Wang and Y. P. Chen, *TrAC, Trends Anal. Chem.*, 2018, **106**, 213–224.
15 D. Liu, T. Tian, X. Chen, Z. Lei, Y. Song, Y. Shi, T. Ji, Z. Zhu, L. Yang and C. Yang, *Analyst*, 2018, **143**, 1294–1304.
16 L. Zhang, B. Ding, Q. Chen, Q. Feng, L. Lin and J. Sun, *TrAC, Trends Anal. Chem.*, 2017, **94**, 106–116.
17 J. Shen, Y. Li, H. Gu, F. Xia and X. Zuo, *Chem. Rev.*, 2014, **114**, 7631–7677.
18 G. Aragay, F. Pino and A. Merkoci, *Chem. Rev.*, 2012, **112**, 5317–5338.
19 M. Pirzada and Z. Altintas, *Chem. Soc. Rev.*, 2022, **51**, 5805–5841.
20 X. Huang, Y. Liu, B. Yung, Y. Xiong and X. Chen, *ACS Nano*, 2017, **11**, 5238–5292.
21 P. Y. You, F. C. Li, M. H. Liu and Y. H. Chan, *ACS Appl. Mater. Interfaces*, 2019, **11**, 9841–9849.
22 S. Ling, M. Dong, Y. Xu, A. Xu, J. Lin, M. Lin, Q. Zhao and S. Wang, *Biosens. Bioelectron.*, 2022, **217**, 114676.
23 Y. Date, A. Aota, S. Terakado, K. Sasaki, N. Matsumoto, Y. Watanabe, T. Matsue and N. Ohmura, *Anal. Chem.*, 2013, **85**, 434–440.
24 J. W. Lim, T. Y. Kim and M. A. Woo, *Biosens. Bioelectron.*, 2021, **183**, 113228.
25 S. Shrivastava, T. Q. Trung and N. E. Lee, *Chem. Soc. Rev.*, 2020, **49**, 1812–1866.
26 D. Mark, S. Haeberle, G. Roth, F. von Stetten and R. Zengerle, *Chem. Soc. Rev.*, 2010, **39**, 1153–1182.
27 H. Yang and M. A. M. Gijs, *Chem. Soc. Rev.*, 2018, **47**, 1391–1458.
28 Y. Yao, X. Chen, X. Zhang, Q. Liu, J. Zhu, W. Zhao, S. Liu and G. Sui, *ACS Sens.*, 2020, **5**, 1354–1362.
29 S. J. Oh, B. H. Park, G. Choi, J. H. Seo, J. H. Jung, J. S. Choi, H. Kim do and T. S. Seo, *Lab Chip*, 2016, **16**, 1917–1926.
30 J. Kim, K. Hong, H. Kim, J. Seo, J. Jeong, P. K. Bae, Y. B. Shin, J. H. Lee, H. J. Oh and S. Chung, *Sens. Actuators, B*, 2020, **316**, 128094.
31 N. K. Khosla, J. M. Lesinski, M. Colombo, L. Bezinge, A. J. deMello and D. A. Richards, *Lab Chip*, 2022, **22**, 3340–3360.
32 S. Maity, S. Ghosh, T. Bhuyan, D. Das and D. Bandyopadhyay, *ACS Sustainable Chem. Eng.*, 2020, **8**, 9268–9276.
33 Z. Gao, Y. Song, T. Y. Hsiao, J. He, C. Wang, J. Shen, A. MacLachlan, S. Dai, B. H. Singer, K. Kurabayashi and P. Chen, *ACS Nano*, 2021, **15**, 18023–18036.
34 E. Hemmig, Y. Temiz, O. Gokce, R. D. Lovchik and E. Delamarche, *Anal. Chem.*, 2020, **92**, 940–946.
35 Q. Lin, J. Wu, X. Fang and J. Kong, *Anal. Chim. Acta*, 2020, **1118**, 18–25.
36 N. M. Pham, S. Rusch, Y. Temiz, H. P. Beck, W. Karlen and E. Delamarche, *Biomed. Microdevices*, 2019, **21**, 24.
37 Z. Feng, S. Zhi, L. Guo, Y. Zhou and C. Lei, *Mikrochim. Acta*, 2019, **186**, 252.
38 W. Hsu, Y. T. Shih, M. S. Lee, H. Y. Huang and W. N. Wu, *Biosensors*, 2022, **12**, 340.
39 A. Kumar, A. Parihar, U. Panda and D. S. Parihar, *ACS Appl. Bio. Mater.*, 2022, **5**, 2046–2068.
40 R. Rodriguez-Moncayo, D. F. Cedillo-Alcantar, P. E. Guevara-Pantoja, O. G. Chavez-Pineda, J. A. Hernandez-Ortiz, J. U. Amador-Hernandez, G. Rojas-Velasco, F. Sanchez-Muñoz, D. Manzur-Sandoval, L. D. Patino-Lopez, D. A. May-Arrioja, R. Posadas-Sanchez,

G. Vargas-Alarcon and J. L. Garcia-Cordero, *Lab Chip*, 2021, **21**, 93–104.
41 D. G. Rackus, M. H. Shamsi and A. R. Wheeler, *Chem. Soc. Rev.*, 2015, **44**, 5320–5340.
42 A. Ahmed, J. V. Rushworth, N. A. Hirst and P. A. Millner, *Clin. Microbiol. Rev.*, 2014, **27**, 631–646.
43 J. Adkins, K. Boehle and C. Henry, *Electrophoresis*, 2015, **36**, 1811–1824.
44 Y. Zhang and X. Chen, *Nanoscale*, 2019, **11**, 19105–19118.
45 W. Wen, X. Yan, C. Zhu, D. Du and Y. Lin, *Anal. Chem.*, 2017, **89**, 138–156.
46 W. W. Zhao, J. J. Xu and H. Y. Chen, *Anal. Chem.*, 2018, **90**, 615–627.
47 Y. Peng, C. Rabin, C. T. Walgama, N. E. Pollok, L. Smith, I. Richards and R. M. Crooks, *ACS Sens.*, 2021, **6**, 1111–1119.
48 L. Cao, J. Cai, W. Deng, Y. Tan and Q. Xie, *Anal. Chem.*, 2020, **92**, 16267–16273.
49 F. G. Ortega, M. D. Regiart, A. Rodriguez-Martinez, D. de Miguel-Perez, M. J. Serrano, J. A. Lorente, G. Tortella, O. Rubilar, K. Sapag, M. Bertotti and M. A. Fernandez-Baldo, *Anal. Chem.*, 2021, **93**, 1143–1153.
50 A. Tarasov, D. W. Gray, M. Y. Tsai, N. Shields, A. Montrose, N. Creedon, P. Lovera, A. O'Riordan, M. H. Mooney and E. M. Vogel, *Biosens. Bioelectron.*, 2016, **79**, 669–678.
51 Y. Chen, W. Duan, L. Xu, G. Li, Y. Wan and H. Li, *Anal. Chim. Acta*, 2022, **1211**, 339904.
52 J. F. Rusling, *Anal. Chem.*, 2013, **85**, 5304–5310.
53 J. Shen, Y. Zhou, F. Fu, H. Xu, J. Lv, Y. Xiong and A. Wang, *Talanta*, 2015, **142**, 145–149.
54 L. D. Xu, Q. Zhang, S. N. Ding, J. J. Xu and H. Y. Chen, *ACS Omega*, 2019, **4**, 21431–21438.
55 A. V. Petrakova, A. E. Urusov, M. K. Gubaydullina, A. V. Bartosh, A. V. Zherdev and B. B. Dzantiev, *Talanta*, 2017, **175**, 77–81.
56 W. B. Shim, M. J. Kim, H. Mun and M. G. Kim, *Biosens. Bioelectron.*, 2014, **62**, 288–294.
57 C. Zhu, G. Zhao and W. Dou, *Sens. Actuators, B*, 2018, **266**, 392–399.
58 M. Moumita, K. M. Shankar, P. B. Abhiman and B. A. Shamasundar, *Food Chem.*, 2019, **270**, 585–592.
59 M. Liu, Y. Li, H. Zheng, Y. Zhou, B. Wang and Z. Hu, *Anal. Methods*, 2015, **7**, 7824–7830.
60 X. Huang, Z. P. Aguilar, H. Xu, W. Lai and Y. Xiong, *Biosens. Bioelectron.*, 2016, **75**, 166–180.
61 A. Hlavacek, Z. Farka, M. Hubner, V. Hornakova, D. Nemecek, R. Niessner, P. Skladal, D. Knopp and H. H. Gorris, *Anal. Chem.*, 2016, **88**, 6011–6017.
62 Y. Zhao, X. Liu, X. Wang, C. Sun, X. Wang, P. Zhang, J. Qiu, R. Yang and L. Zhou, *Talanta*, 2016, **161**, 297–303.
63 Y. Wang, Q. Zhang, W. Yuan, Y. Wang, H. J. Loghry, Z. Zhao, M. J. Kimber, L. Dong and M. Lu, *Lab Chip*, 2021, **21**, 196–204.
64 E. Bidram, Y. Esmaeili, A. Amini, R. Sartorius, F. R. Tay, L. Shariati and P. Makvandi, *ACS Biomater. Sci. Eng.*, 2021, **7**, 2150–2176.
65 S. Eissa, H. A. Alhadrami, M. Al-Mozaini, A. M. Hassan and M. Zourob, *Mikrochim. Acta*, 2021, **188**, 199.
66 Z. Wang, Z. Zheng, H. Hu, Q. Zhou, W. Liu, X. Li, Z. Liu, Y. Wang and Y. Ma, *Lab Chip*, 2020, **20**, 4255–4261.
67 X. Mao, Y. Ma, A. Zhang, L. Zhang, L. Zeng and G. Liu, *Anal. Chem.*, 2009, **81**, 1660–1668.
68 E. G. Rey, D. O'Dell, S. Mehta and D. Erickson, *Anal. Chem.*, 2017, **89**, 5095–5100.
69 C. Qin, W. Wen, X. Zhang, H. Gu and S. Wang, *Chem. Commun.*, 2015, **51**, 8273–8275.
70 L. Guo, X. Wu, L. Liu, H. Kuang and C. Xu, *Small*, 2018, **14**, 1701782.
71 I. H. Lee, J. M. Lee and Y. Jung, *ACS Appl. Mater. Interfaces*, 2014, **6**, 7659–7664.
72 Z. Farka, T. Jurik, D. Kovar, L. Trnkova and P. Skladal, *Chem. Rev.*, 2017, **117**, 9973–10042.
73 P. Brangel, A. Sobarzo, C. Parolo, B. S. Miller, P. D. Howes, S. Gelkop, J. J. Lutwama, J. M. Dye, R. A. McKendry, L. Lobel and M. M. Stevens, *ACS Nano*, 2018, **12**, 63–73.
74 Z. Shen, Y. Luo, Q. Wang, X. Wang and R. Sun, *ACS Appl. Mater. Interfaces*, 2014, **6**, 16147–16155.
75 W. Kim, Y. H. Kim, H. K. Park and S. Choi, *ACS Appl. Mater. Interfaces*, 2015, **7**, 27910–27917.
76 C. Muehlethaler, M. Leona and J. R. Lombardi, *Anal. Chem.*, 2016, **88**, 152–169.
77 O. Tokel, F. Inci and U. Demirci, *Chem. Rev.*, 2014, **114**, 5728–5752.
78 A. Pollap and P. Swit, *Int. J. Mol. Sci.*, 2022, **23**, 4740.
79 V. Tran, B. Walkenfort, M. Konig, M. Salehi and S. Schlucker, *Angew. Chem., Int. Ed. Engl.*, 2019, **58**, 442–446.
80 M. J. Bistaffa, S. A. Camacho, W. M. Pazin, C. J. L. Constantino, O. N. Oliveira, Jr. and P. H. B. Aoki, *Talanta*, 2022, **244**, 123381.
81 C. Wang, C. Wang, X. Wang, K. Wang, Y. Zhu, Z. Rong, W. Wang, R. Xiao and S. Wang, *ACS Appl. Mater. Interfaces*, 2019, **11**, 19495–19505.
82 J. Turkevich, P. C. Stevenson and J. Hillier, *Discuss. Faraday Soc.*, 1951, **11**, 55.
83 X. Ji, X. Song, J. Li, Y. Bai, W. Yang and X. Peng, *J. Am. Chem. Soc.*, 2007, **129**, 13939–13948.
84 G. Frens, *Nat. Phys. Sci.*, 1973, **241**, 20–22.
85 K. L. Kelly, E. Coronado, L. L. Zhao and G. C. Schatz, *J. Phys. Chem. B*, 2003, **107**, 668–677.
86 M. Faraday, *Philos. Trans. R. Soc. London*, 1857, **147**, 145–181.
87 N. Khlebtsov and L. Dykman, *Chem. Soc. Rev.*, 2011, **40**, 1647–1671.
88 J. Sun, Y. Xianyu and X. Jiang, *Chem. Soc. Rev.*, 2014, **43**, 6239–6253.
89 T. Kim, K. Lee, M. S. Gong and S. W. Joo, *Langmuir*, 2005, **21**, 9524–9528.
90 H. M. Zakaria, A. Shah, M. Konieczny, J. A. Hoffmann, A. J. Nijdam and M. E. Reeves, *Langmuir*, 2013, **29**, 7661–7673.
91 D. Liu, W. Qu, W. Chen, W. Zhang, Z. Wang and X. Jiang, *Anal. Chem.*, 2010, **82**, 9606–9610.
92 S. F. Chou, *Analyst*, 2013, **138**, 2620–2623.
93 J. W. Park and J. S. Shumaker-Parry, *ACS Nano*, 2015, **9**, 1665–1682.

94 C. Burda, X. Chen, R. Narayanan and M. A. El-Sayed, *Chem. Rev.*, 2005, **105**, 1025–1102.
95 W. Zhou, X. Gao, D. Liu and X. Chen, *Chem. Rev.*, 2015, **115**, 10575–10636.
96 L. Zhang, Y. Huang, J. Wang, Y. Rong, W. Lai, J. Zhang and T. Chen, *Langmuir*, 2015, **31**, 5537–5544.
97 M. Wu, H. Li, Y. Jiang, C. Song, H. Guo, S. Wu, C. Liu, J. Li, H. Zeng, X. Zhai, W. Zhang, E. Fan and Q. Liu, *Analyst*, 2015, **140**, 6595–6601.
98 Y. Gao, X.-Y. Meng, H. Zhang, Y. Luo, Y. Sun, Y. Li, M. Abid and H.-J. Qiu, *Sens. Actuators, B*, 2018, **274**, 304–309.
99 S. Y. Hou, Y. L. Hsiao, M. S. Lin, C. C. Yen and C. S. Chang, *Talanta*, 2012, **99**, 375–379.
100 N. Hildebrandt, C. M. Spillmann, W. R. Algar, T. Pons, M. H. Stewart, E. Oh, K. Susumu, S. A. Diaz, J. B. Delehanty and I. L. Medintz, *Chem. Rev.*, 2017, **117**, 536–711.
101 J. W. Zhou, X. M. Zou, S. H. Song and G. H. Chen, *J. Agric. Food Chem.*, 2018, **66**, 1307–1319.
102 X. Michalet, F. F. Pinaud, L. A. Bentolila, J. M. Tsay, S. Doose, J. J. Li, G. Sundaresan, A. M. Wu, S. S. Gambhir and S. Weiss, *Science*, 2005, **307**, 538–544.
103 W. C. W. C. a. S. Nie, *Science*, 1998, **281**, 2016–2018.
104 Z. Rong, Q. Wang, N. Sun, X. Jia, K. Wang, R. Xiao and S. Wang, *Anal. Chim. Acta*, 2019, **1055**, 140–147.
105 H. Duan, X. Huang, Y. Shao, L. Zheng, L. Guo and Y. Xiong, *Anal. Chem.*, 2017, **89**, 7062–7068.
106 Z. Li, Y. Wang, J. Wang, Z. Tang, J. G. Pounds and Y. Lin, *Anal. Chem.*, 2010, **82**, 7008–7014.
107 J. Wang, H.-M. Meng, J. Chen, J. Liu, L. Zhang, L. Qu, Z. Li and Y. Lin, *ACS Omega*, 2019, **4**, 6789–6795.
108 X. Li, W. Li, Q. Yang, X. Gong, W. Guo, C. Dong, J. Liu, L. Xuan and J. Chang, *ACS Appl. Mater. Interfaces*, 2014, **6**, 6406–6414.
109 J. Hu, Z. L. Zhang, C. Y. Wen, M. Tang, L. L. Wu, C. Liu, L. Zhu and D. W. Pang, *Anal. Chem.*, 2016, **88**, 6577–6584.
110 X. Guo, F. Wen, N. Zheng, Q. Luo, H. Wang, H. Wang, S. Li and J. Wang, *Biosens. Bioelectron.*, 2014, **56**, 340–344.
111 M. Ren, H. Xu, X. Huang, M. Kuang, Y. Xiong, H. Xu, Y. Xu, H. Chen and A. Wang, *ACS Appl. Mater. Interfaces*, 2014, **6**, 14215–14222.
112 K. Xiao, K. Wang, W. Qin, Y. Hou, W. Lu, H. Xu, Y. Wo and D. Cui, *Talanta*, 2017, **164**, 463–469.
113 T. Ma, Y. Hou, J. Zeng, C. Liu, P. Zhang, L. Jing, D. Shangguan and M. Gao, *J. Am. Chem. Soc.*, 2018, **140**, 211–218.
114 V. Nabaei, R. Chandrawati and H. Heidari, *Biosens. Bioelectron.*, 2018, **103**, 69–86.
115 Q. Zhang, L. Li, Z. Qiao, C. Lei, Y. Fu, Q. Xie, S. Yao, Y. Li and Y. Ying, *Anal. Chem.*, 2017, **89**, 12145–12151.
116 M. K. Masud, J. Na, M. Younus, M. S. A. Hossain, Y. Bando, M. J. A. Shiddiky and Y. Yamauchi, *Chem. Soc. Rev.*, 2019, **48**, 5717–5751.
117 C. Liu, Q. Jia, C. Yang, R. Qiao, L. Jing, L. Wang, C. Xu and M. Gao, *Anal. Chem.*, 2011, **83**, 6778–6784.
118 B. Zhang, W. Ma, F. Li, W. Gao, Q. Zhao, W. Peng, J. Piao, X. Wu, H. Wang, X. Gong and J. Chang, *Nanoscale*, 2017, **9**, 18711–18722.
119 J. Chen, L. Hao, Y. Wu, T. Lin, X. Li, Y. Leng, X. Huang and Y. Xiong, *Chem. Commun.*, 2019, **55**, 10312–10315.
120 M. A. Nash, J. N. Waitumbi, A. S. Hoffman, P. Yager and P. S. Stayton, *ACS Nano*, 2012, **6**, 6776–6785.
121 Y. Chen, Y. Xianyu, J. Wu, M. Dong, W. Zheng, J. Sun and X. Jiang, *Anal. Chem.*, 2017, **89**, 5422–5427.
122 X. Liu, C. Zhang, K. Liu, H. Wang, C. Lu, H. Li, K. Hua, J. Zhu, W. Hui, Y. Cui and X. Zhang, *Anal. Chem.*, 2018, **90**, 3430–3436.
123 A. Ramanaviciene, A. Popov, E. Baliunaite, B. Brasiunas, A. Kausaite-Minkstimiene, U. Tamer, G. Kirdaite, E. Bernotiene and A. Mobasheri, *Biosensors*, 2022, **12**, 65.
124 S. Oh, J. Kim, V. T. Tran, D. K. Lee, S. R. Ahmed, J. C. Hong, J. Lee, E. Y. Park and J. Lee, *ACS Appl. Mater. Interfaces*, 2018, **10**, 12534–12543.
125 M. E. Cortina, L. J. Melli, M. Roberti, M. Mass, G. Longinotti, S. Tropea, P. Lloret, D. A. R. Serantes, F. Salomon, M. Lloret, A. J. Caillava, S. Restuccia, J. Altcheh, C. A. Buscaglia, L. Malatto, J. E. Ugalde, L. Fraigi, C. Moina, G. Ybarra, A. E. Ciocchini and D. J. Comerci, *Biosens. Bioelectron.*, 2016, **80**, 24–33.
126 D. Liu, S. Jia, H. Zhang, Y. Ma, Z. Guan, J. Li, Z. Zhu, T. Ji and C. J. Yang, *ACS Appl. Mater. Interfaces*, 2017, **9**, 22252–22258.
127 T. Jiang, Y. Song, D. Du, X. Liu and Y. Lin, *ACS Sens.*, 2016, **1**, 717–724.
128 M. S. Kim, S. H. Kweon, S. Cho, S. S. A. An, M. I. Kim, J. Doh and J. Lee, *ACS Appl. Mater. Interfaces*, 2017, **9**, 35133–35140.
129 T. Jiang, Y. Song, T. Wei, H. Li, D. Du, M. J. Zhu and Y. Lin, *Biosens. Bioelectron.*, 2016, **77**, 687–694.
130 L. Liang, L. Jin, Y. Ran, L.-P. Sun and B.-O. Guan, *Anal. Chem.*, 2018, **90**, 10851–10857.
131 H. Afsharan, F. Navaeipour, B. Khalilzadeh, H. Tajalli, M. Mollabashi, M. J. Ahar and M.-R. Rashidi, *Biosens. Bioelectron.*, 2016, **80**, 146–153.
132 Y. Chen, J. Sun, Y. Xianyu, B. Yin, Y. Niu, S. Wang, F. Cao, X. Zhang, Y. Wang and X. Jiang, *Nanoscale*, 2016, **8**, 15205–15212.
133 D. Huang, B. Lin, Y. Song, Z. Guan, J. Cheng, Z. Zhu and C. Yang, *ACS Appl. Mater. Interfaces*, 2019, **11**, 1800–1806.
134 Q. Fu, Z. Wu, D. Du, C. Zhu, Y. Lin and Y. Tang, *ACS Sens.*, 2017, **2**, 789–795.
135 L. Shi, J. Lei, B. Zhang, B. Li, C. J. Yang and Y. Jin, *ACS Appl. Mater. Interfaces*, 2018, **10**, 12526–12533.
136 X. Yin, L. Liang, P. Zhao, F. Lan, L. Zhang, S. Ge and J. Yu, *J. Mater. Chem. B*, 2018, **6**, 5795–5801.
137 Z. Zhang, S. Shikha, J. Liu, J. Zhang, Q. Mei and Y. Zhang, *Anal. Chem.*, 2019, **91**, 548–568.
138 G. Chen, H. Qiu, P. N. Prasad and X. Chen, *Chem. Rev.*, 2014, **114**, 5161–5214.
139 R. Gao, C. Hao, L. Xu, C. Xu and H. Kuang, *Anal. Chem.*, 2018, **90**, 5414–5421.

140 F. Hou, H. Liu, Y. Zhang, Z. Gao, S. Sun, Y. Tang and H. Guo, *New J. Chem.*, 2020, **44**, 15498–15506.
141 Z. Liang, X. Wang, W. Zhu, P. Zhang, Y. Yang, C. Sun, J. Zhang, X. Wang, Z. Xu, Y. Zhao, R. Yang, S. Zhao and L. Zhou, *ACS Appl. Mater. Interfaces*, 2017, **9**, 3497–3504.
142 Y. Chen, Q. Chen, M. Han, J. Liu, P. Zhao, L. He, Y. Zhang, Y. Niu, W. Yang and L. Zhang, *Biosens. Bioelectron.*, 2016, **79**, 430–434.
143 P. Zhang, X. Liu, C. Wang, Y. Zhao, F. Hua, C. Li, R. Yang and L. Zhou, *PLoS One*, 2014, **9**, e105305.
144 J. Kim, J. H. Kwon, J. Jang, H. Lee, S. Kim, Y. K. Hahn, S. K. Kim, K. H. Lee, S. Lee, H. Pyo, C. S. Song and J. Lee, *Biosens. Bioelectron.*, 2018, **112**, 209–215.
145 T. Ji, X. Xu, X. Wang, Q. Zhou, W. Ding, B. Chen, X. Guo, Y. Hao and G. Chen, *Sens. Actuators, B*, 2019, **282**, 309–316.
146 W. Hong, L. Huang, H. Wang, J. Qu, Z. Guo, C. Xie, Z. Zhu, Y. Zhang, Z. Du, Y. Yan, Y. Zheng, H. Huang, R. Yang and L. Zhou, *J. Microbiol. Methods*, 2010, **83**, 133–140.
147 M. K. Tsang, W. Ye, G. Wang, J. Li, M. Yang and J. Hao, *ACS Nano*, 2016, **10**, 598–605.
148 C. Song, A. Zhi, Q. Liu, J. Yang, G. Jia, J. Shervin, L. Tang, X. Hu, R. Deng, C. Xu and G. Zhang, *Biosens. Bioelectron.*, 2013, **50**, 62–65.
149 L. Huang, T. Liao, J. Wang, L. Ao, W. Su and J. Hu, *Adv. Funct. Mater.*, 2018, **28**, 1705380.
150 X. Yang, X. Liu, B. Gu, H. Liu, R. Xiao, C. Wang and S. Wang, *Microchim. Acta*, 2020, **187**, 570.
151 L. Huang, J. Jin, J. Wang, C. Jiang, M. Xu, H. Wen, T. Liao and J. Hu, *Nanoscale*, 2019, **11**, 16026–16035.
152 J. Zhou, M. Ren, W. Wang, L. Huang, Z. Lu, Z. Song, M. F. Foda, L. Zhao and H. Han, *Anal. Chem.*, 2020, **92**, 8802–8809.
153 W. R. Algar, D. Wegner, A. L. Huston, J. B. Blanco-Canosa, M. H. Stewart, A. Armstrong, P. E. Dawson, N. Hildebrandt and I. L. Medintz, *J. Am. Chem. Soc.*, 2012, **134**, 1876–1891.
154 D. Wang, Z. Zhang, P. Li, Q. Zhang, X. Ding and W. Zhang, *J. Agric. Food Chem.*, 2015, **63**, 10313–10318.
155 Q. You, M. Liu, Y. Liu, H. Zheng, Z. Hu, Y. Zhou and B. Wang, *ACS Sens.*, 2017, **2**, 569–575.
156 F.-B. Wu, S.-Q. Han, C. Zhang and Y.-F. He, *Anal. Chem.*, 2002, **74**, 5882–5889.
157 B. Qiao, Y. Li, P. Hu, Y. Sun, Z. Si, S. Lu, H. Ren, Z. Liu, Y. Zhang, L. Meng and Y. Zhou, *Sens. Actuators, B*, 2018, **262**, 221–227.
158 F. Hou, M. Bai, Y. Zhang, H. Liu, S. Sun and H. Guo, *Microchem. J.*, 2020, **155**, 104690.
159 K. Y. Xing, J. Peng, D. F. Liu, L. M. Hu, C. Wang, G. Q. Li, G. G. Zhang, Z. Huang, S. Cheng, F. F. Zhu, N. M. Liu and W. H. Lai, *Anal. Chim. Acta*, 2018, **998**, 52–59.
160 Y. Yao, W. Guo, J. Zhang, Y. Wu, W. Fu, T. Liu, X. Wu, H. Wang, X. Gong, X. J. Liang and J. Chang, *ACS Appl. Mater. Interfaces*, 2016, **8**, 22963–22970.
161 Y. Chen, Y. Cao, C. Ma and J.-J. Zhu, *Mater. Chem. Front.*, 2020, **4**, 369–385.
162 L.-D. Xu, F.-L. Du, J. Zhu and S.-N. Ding, *Analyst*, 2021, **146**, 706–713.
163 B. J. Brownlee, J. C. Claussen and B. D. Iverson, *ACS Appl. Nano Mater.*, 2020, **3**, 10166–10175.
164 X. Liu, Z. Cheng, H. Fan, S. Ai and R. Han, *Electrochim. Acta*, 2011, **56**, 6266–6270.
165 Z. Jia, Y. Ma, L. Yang, C. Guo, N. Zhou, M. Wang, L. He and Z. Zhang, *Biosens. Bioelectron.*, 2019, **133**, 55–63.
166 J. Lee, S. R. Ahmed, S. Oh, J. Kim, T. Suzuki, K. Parmar, S. S. Park, J. Lee and E. Y. Park, *Biosens. Bioelectron.*, 2015, **64**, 311–317.
167 H. Teymourian, A. Barfidokht and J. Wang, *Chem. Soc. Rev.*, 2020, **49**, 7671–7709.
168 N. Singh, M. A. Ali, P. Rai, I. Ghori, A. Sharma, B. D. Malhotra and R. John, *Lab Chip*, 2020, **20**, 760–777.
169 G. Seo, G. Lee, M. J. Kim, S. H. Baek, M. Choi, K. B. Ku, C. S. Lee, S. Jun, D. Park, H. G. Kim, S. J. Kim, J. O. Lee, B. T. Kim, E. C. Park and S. I. Kim, *ACS Nano*, 2020, **14**, 5135–5142.
170 F. Liu, Y. H. Kim, D. S. Cheon and T. S. Seo, *Sens. Actuators, B*, 2013, **186**, 252–257.
171 A. Molinero-Fernandez, M. A. Lopez and A. Escarpa, *Anal. Chem.*, 2020, **92**, 5048–5054.
172 A. Sangili, T. Kalyani, S.-M. Chen, A. Nanda and S. K. Jana, *ACS Appl. Bio Mater.*, 2020, **3**, 7620–7630.
173 Y. Wang, Y. Hu, Q. He, J. Yan, H. Xiong, N. Wen, S. Cai, D. Peng, Y. Liu and Z. Liu, *Biosens. Bioelectron.*, 2020, **169**, 112604.
174 G.-H. Qiu, Z.-H. Weng, P.-P. Hu, W.-J. Duan, B.-P. Xie, B. Sun, X.-Y. Tang and J.-X. Chen, *Talanta*, 2018, **180**, 396–402.
175 N. A. S. Omar, Y. W. Fen, S. Saleviter, Y. M. Kamil, W. M. E. M. M. Daniyal, J. Abdullah and M. A. Mahdi, *Sens. Actuators, A*, 2020, **303**, 111830.
176 K. Ghanbari and M. Roushani, *Sens. Actuators, B*, 2018, **258**, 1066–1071.
177 J. Chen, H. Meng, Y. Tian, R. Yang, D. Du, Z. Li, L. Qu and Y. Lin, *Nanoscale Horiz.*, 2019, **4**, 321–338.
178 J. Chen, Z. Huang, H. Meng, L. Zhang, D. Ji, J. Liu, F. Yu, L. Qu and Z. Li, *Sens. Actuators, B*, 2018, **260**, 770–777.
179 W. Gao, Z. Liu, L. Qi, J. Lai, S. A. Kitte and G. Xu, *Anal. Chem.*, 2016, **88**, 7654–7659.
180 T. Cai, Y. Liu, L. Wang, S. Zhang, J. Ma, W. Dong, Y. Zeng, J. Yuan, C. Liu and S. Luo, *ACS Appl. Mater. Interfaces*, 2018, **10**, 25350–25359.
181 X. Ren, J. Yan, D. Wu, Q. Wei and Y. Wan, *ACS Sens.*, 2017, **2**, 1267–1271.
182 A. Xiao, Y. Huang, J. Zheng, P. Chen and B. O. Guan, *ACS Appl. Mater. Interfaces*, 2020, **12**, 1799–1805.
183 R. S. Fernandes, J. de Oliveira Silva, K. B. Gomes, R. B. Azevedo, D. M. Townsend, A. de Paula Sabino and A. L. Branco de Barros, *Biomed. Pharmacother.*, 2022, **153**, 113538.
184 K. Wang, X. Xing, Y. Ding, W. Guo, X. Hong and H. Zhao, *Biosens. Bioelectron.*, 2020, **150**, 111870.
185 K. M. Byers, A. R. Bird, H. D. Cho and J. C. Linnes, *ACS Omega*, 2020, **5**, 4673–4681.
186 M. Shen, N. Li, Y. Lu, J. Cheng and Y. Xu, *Lab Chip*, 2020, **20**, 2626–2634.

187 X. Zhu, M. Sarwar, J. J. Zhu, C. Zhang, A. Kaushik and C. Z. Li, *Biosens. Bioelectron.*, 2019, **126**, 690–696.
188 S. Sachdeva, R. W. Davis and A. K. Saha, *Front. Bioeng. Biotechnol.*, 2020, **8**, 602659.
189 A. Rubio-Monterde, D. Quesada-Gonzalez and A. Merkoci, *Anal. Chem.*, 2023, **95**, 468–489.
190 S. Yadav, M. A. Sadique, P. Ranjan, N. Kumar, A. Singhal, A. K. Srivastava and R. Khan, *ACS Appl. Bio Mater.*, 2021, **4**, 2974–2995.
191 S. K. Vashist, P. B. Luppa, L. Y. Yeo, A. Ozcan and J. H. T. Luong, *Trends Biotechnol.*, 2015, **33**, 692–705.
192 Q. Song, X. Sun, Z. Dai, Y. Gao, X. Gong, B. Zhou, J. Wu and W. Wen, *Lab Chip*, 2021, **21**, 1634–1660.
193 J. Walter-Weingartner, M. Bergmann, K. Weber, U. Truyen, C. Muresan and K. Hartmann, *Viruses*, 2021, **13**, 2080.